2016

3D printing PhycoTrix™ for wound healing

Jeremy Nicolas Dinoro
University of Wollongong

3D PRINTING PHYCOTRIX™
FOR WOUND HEALING

By

JEREMY NICOLAS DINORO

Bachelor of Science (Medical Biotechnology)

This thesis is presented as part of the requirements for the award of

MASTER OF PHILOSOPHY

from

UNIVERSITY OF WOLLONGONG

AUSTRALIAN INSTITUTE OF INNOVATIVE MATERIALS
INTELLIGENT POLYMER RESEARCH INSTITUTE

AUGUST 2016

CERTIFICATION

I, Jeremy Nicolas Dinoro, declare that this dissertation, submitted in conjunction with the required coursework is in fulfilment for awarding the degree of Master of Philosophy, within the AIIM Faculty at the Intelligent Polymer Research Institute, University of Wollongong, is my work unless referenced, acknowledged or stated otherwise. This document has not been submitted for qualifications at any other academic institution.

Jeremy Nicolas Dinoro

August 22nd, 2016

ACKNOWLEDGEMENTS

First and foremost I would like to thank my academic supervisors, in particular, my supervisor Dr Zhilian Yue for her ongoing encouragement, support, and guidance, I truly value everything you have done. Also Dr Stephen Beirne and Prof. Gordon Wallace for their invaluable perspicacity. To all those involved in establishing the International Biofabrication Master's degree, your efforts are greatly appreciated.

A significant portion of this work would not have been achievable without the deep insight from fellow students and colleagues at the Wollongong University's Innovation Campus (IC) – both the Intelligent Polymer Research Institute (IPRI) and Australian National Fabrication Facility (ANFF) - within the Australian Institute for Innovative Materials Centre (AIIM) - to everyone, you know who you are, I thank you (and sorry about all the acronyms).

In no specific order, I would like to thank Dr Sina Naficy, Malachy Maher, Dr Hai Xin, Dr Patricia Hayes, Adam Taylor, Chris Richards, Ali Jeiranikhameneh, Dr Cormack Fay, Tobias Soper, Dr Cody Wright, Dr Kati Schirmer and Dr Robert Murphy for their expertise with all the tools and training involved in this work.

This work was also completed in conjunction with Associate Professor Chris Baker, a Melbourne-based Dermatologist. I'd like to acknowledge the contributions he has made, in particular, for real world applications. Along with the ARC Centre of Excellence for Electromaterials Science Australian Reseach Centre for the opportunity to pursue the research.

Additionally, the seaweed extract, PhycoTrix™, was supplied by a local company Venus Shell Systems Pty Ltd. I'd like to thank the whole team involved in the cultivation and extraction, primarily its founder, director and chief operating officer Dr Pia Winberg for her collaborative efforts, the supply of the material, and her thorough understanding of each facet.

And finally my family and friends, my cousin Diandra Mauriello and Dr. Michael De Santis for somehow proofreading this and especially my Mum and Dad, who have supported me through everything and without which I would not have made it this far.

ABSTRACT

With the advent of additive manufacturing and its recent use in regenerative medicine, bioprinting has become a promising technology for tissue engineering applications. PhycoTrix™, a sulphated marine-derived polysaccharide, taken from the cell wall of a DNA barcoded green algal spp., (Chlorophyta), has a chemical structure similar to mammalian glycosaminoglycans found within the dermal skin layer extracellular matrix. This sustainable, under-utilised source of biomaterial was developed into a bio-ink for use in bioprinting. Specifically, a dual-network hydrogel was engineered through ionic and chemical means. This hydrogel was characterised following methacrylation through ^{1}H NMR, FT-IR, and circular dichroism. The physical properties, printability, and crosslinking kinetics were all assessed through rheology and mechanical properties through micro-indentation. Preliminary cytocompatibility studies were evaluated using fibroblasts and adipose-derived stem cells. The results indicated relatively high cell binding affinity and proliferation compared to other alginate studies, suggesting this novel biomaterial could be useful for wound healing applications, such as wound dressings and matrices for tissue repair and regeneration.

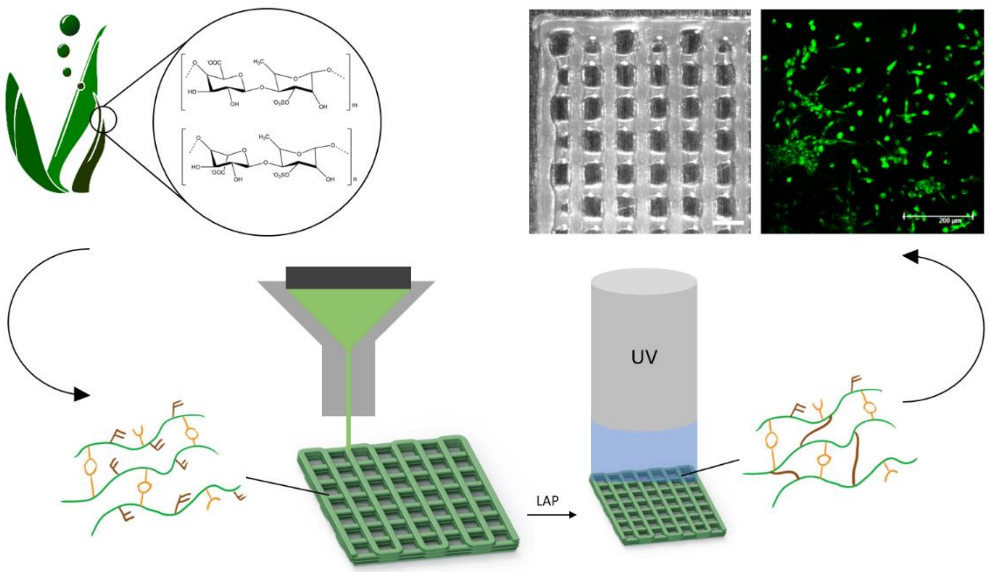

Figure 1 | Graphical abstract showing the bioink development from algal origin.

CONTENTS

ABBREVIATIONS

AM – Additive Manufacturing

TE – Tissue Engineering

ECM – Extra Cellular Matrix

GAG (s) – Glycosaminoglycan (s)

PT - PhycoTrix ™

PTMA – PhycoTrix ™ Methacrylate

MA – Methacrylic Anhydride

MWCO – Molecular Weight Cut Off

DI – De-ionised

ICE – Ionic-Covalent Entanglement

IPN – Interpenetrating Polymer Network

DN – Double Network

LVE – Linear Viscoelastic region

SD – Standard Deviation

VEGF – Vascular Endothelial Growth Factor

BM – Basement Membrane

FGF – Fibroblast Growth Factor

KC (s) – Keratinocytes

ALI - Air-Liquid-Interface

VSS – Venus Shell Systems Pty Ltd

1 INTRODUCTION

1.1 Outline

To address the multidisciplinary nature of biofabrication, this work has been introduced in three main sections. Firstly the problem at hand of wound healing and skin tissue regeneration is outlined, from an anatomical and physiological perspective, with emphasis on current treatments. Secondly, the study focuses on various additive manufacturing approaches, in the context of bioprinting. The use of biomaterial-based hydrogels in bioprinting will be described, concentrating on their mechnical and chemical characteristics. The latter section proposes the aims and hypotheses of this work.

1.2 Overview

Additive manufacturing (AM) or 3D printing, coupled with recent advances in tissue engineering (TE) has led to bioprinting and biofabrication. These fields offer great potential in regenerative medicine applications, from printing tissue constructs to the development of complete vascularised organs (Murphy and Atala, 2014). One major advantage of biofabrication includes the precise placement of biomaterials to ensure optimal spatial distribution and mechanical stability. Biofabrication can be used in wound healing, skin tissue repair and developing *de novo* organs (Bartolo *et al.*, 2013, Murphy and Atala, 2014). The creation of biomaterial or hydrogel-based wound healing scaffolds can enhance cell to cell interactions, facilitating an appropriate natural response to trauma (Gao *et al.*, 2006). Biomaterial-based hydrogels can be engineered from natural polymers including those derived from marine polysaccharides such as alginate from brown seaweed, carrageenan from red seaweed and PT from green seaweed (Khalil and Sun, 2009, Dash *et al.*, 2014, Morelli and Chiellini, 2010). These sustainable polysaccharides offer desirable biological and physiochemical qualities suitable for biofabrication (Morelli and Chiellini, 2010, Hachet *et al.*, 2012, Draget *et al.*, 1997).

1.3 The skin

To understand wound healing and skin bioprinting, we must first look at the structural components of the skin. The skin is the largest organ of the body in invertebrates and is a vital external defence against collisions, chemicals, UV-radiation, temperature, and pathogens, among other biological stresses (Clark *et al.*, 2007, Tobin, 2006). Human skin consists of three principal layers: the epidermis, dermis, and hypodermis (Figure 2). The latter is composed of connective tissue and fats, specifically collagen and adipose tissue. These play a fundamental role in the maintenance of homoeostasis and thermoregulation (Metcalfe and Ferguson, 2007a). The dermal layer houses several extracellular matrix (ECM) components including collagen (type I and III) with elastin, various glycosaminoglycans (GAGs) and fibroblasts, all vital in the wound healing response (Böttcher-Haberzeth *et al.*, 2010). Connecting the dermis to the superficial epidermal layer is the basement membrane (BM). The BM acts as an antigen template, enabling the remodelling of damaged skin in vitro (Ralston, 1999). Lastly, the epidermal layer serves to protect the dermal layer, which houses nerves and blood vessels along with other vital ECM components, preventing moisture loss and pathogen entry (Singh *et al.*, 2012).

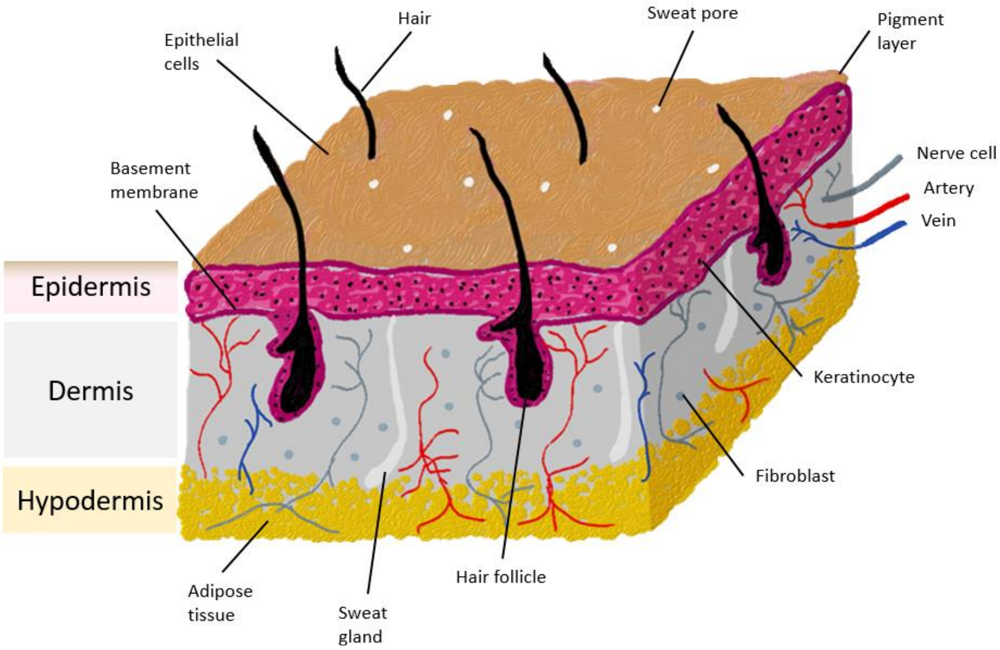

Figure 2 | A basic illustration of the structure of human skin.

1.3.1 Wounds

The burden of chronic wounds on the Australian Health Care System has been estimated to cost up to $2.85 billion annually (Graves and Zheng, 2014). The annual global encumbrance of burns is impacting over 11 million people (Peck, 2011). Attached to this are the indirect costs associated with further wound management with accountability dwelling on the broader healthcare system. This burden ranges from impacts on clinicians, nurses, hospitals, aged care and the individuals, among others.

There are several circumstances under which the protection of the skin can be compromised. These include trauma, chronic ulcers, tumours, burns along with various other dermatological conditions (Dai *et al.*, 2004). Once compromised, the body's wound healing cascade is triggered, generally involving inflammation, proliferation, angiogenesis and remodelling (Park and Barbul, 2004).

Inflammation is initiated by cytokines along with inflammatory mediators such as histamine which cause vasodilation, activate complement and attract macrophages through fibrin (Hunt, 1988, Sinno and Prakash, 2013, Cazander *et al.*, 2012). Thrombin and collagen activate platelets, stimulating the proliferation of growth factors, namely, fibroblast growth factor (FGF) and vascular endothelial cells (Park and Barbul, 2004). Angiogenesis promotes the restoration of blood supply to the regenerating tissues through angiogenic mediators including vascular endothelial growth factor (VEGF) and fibroblast growth factor-2 (FGF-2) (Crowther *et al.*, 2001, Swift *et al.*, 1999). Lastly, apoptosis destroys redundant cells and collagen fibres, glycosaminoglycans (GAGs). This is followed by the remodelling of fibronectin, partially reconstructing the wound site (Cazander *et al.*, 2012).

1.3.2 Wound Dressings and Skin Grafts

A substantial development in wound care was established in a study by Winter (1962), who found that wound re-epithelization was twice as fast when moisture was kept beneath an occlusive dressing. Following initial trauma, when exposed to air, a wound will develop a dry scab, hindering the migration of epidermal cells and keratinocytes (KCs) to the area, prolonging the healing process (Paul and Sharma, 2004). Moist healing provides a workaround, facilitating cell migration, and reducing overall scar formation through exudate absorption and wound insulation (Paul and Sharma, 2004, Atiyeh *et al.*, 2002, Eming *et al.*, 2007). Furthermore, through mimicking the epidermis, a moist environment can reduce pain, increase oxygen delivery, and improve overall cell-to-cell electrochemical interactions (Field and Kerstein, 1994).

Modern wound dressings can be divided into two general groups; inert or passive and interactive or bioactive (Weller and Sussman, 2006). In recent years, with greater insights into wound management, there has been a shift from passive to active wound management (Field and Kerstein, 1994). Inert gauzes are now predominantly used as secondary dressings, that is, they are used as support for interactive dressings. Bioactive dressings interact with the wound site to optimise healing, which includes, but is not limited to, hydrogels, hydrocolloids, iodine dressings along with highly absorbant, hemostatic dressings such as alginate and chitosan-based dressings.

Integrating established wound management strategies with modern technology such as biofabrication can assist in creating new types of dressings and synthetic skin substitutes. Kirker *et al.* (2004) demonstrated that the introduction of crosslinked GAG hydrogel films beneath an occlusive dressing resulted in accelerated wound healing. This has led to an increased interest in developing new occlusive, hydrocolloid, and hydrogel based wound management strategies by clinicians and researchers alike. Additionally, recent advances in skin tissue engineering have brought forward the possibility of artificial skin substitutes.

It is well understood that in the event of skin trauma, particularly burns, immediate protection is essential to prevent infection (Breasted, 1930). Skin grafts such as autografts are still the most common treatment for severe burns. In general, an autograft requires the surgical removal of skin from another part of an individual's body, which is then stretched and applied to the burn site. This method is limited by the availability of sites and leads, of course, to further trauma, potentially resulting in additional complications. Alternative measures with xenografts, allografts and even artificial skin have been explored to transcend autograft limitations (Chardack *et al.*, 1962, Bondoc and Burke, 1971, Yannas and Burke, 1980).

Xenografts are skin grafts from separate species, of which porcine skin is most commonly used, whereas allografts are decellularised cadaveric skin. A study comparing human fibroblast migration and penetration in porcine xenografts against human allografts showed the latter to be more efficient (Armour *et al.*, 2006). The decellularised allograft resulted in an over eighty percent fibroblast infiltration when compared to the approximately thirty percent in the xenograft. Additionally, since xenografts are derived from animals, they pose greater ethical and immunological concerns (Robson *et al.*, 1999, Platt *et al.*, 1991, Miyagawa *et al.*, 1988, Adler *et al.*, 2011).

1.3.3 Skin Tissue Engineering

Engineered skin offers an alternative approach to skin grafts for severe burns and chronic wounds (MacNeil, 2007). The ultimate goal of tissue engineering is to restore the natural structures and functions of tissue constructs by recapitulating key features in the native cellular and tissue microenvironments. The majority of studies into skin tissue engineering concentrate on recreating the dermal and epidermal layers through the use of fibroblasts and keratinocytes (Metcalfe and Ferguson, 2007b).

A fundamental association often overlooked in skin tissue engineering is the influence of hair follicles in skin regeneration (Paus and Cotsarelis, 1999). To develop biofabricated skin, the role of each component in the native construct must be examined with a fine-tooth comb. The skin is mainly composed of adipose tissue, keratinocytes and fibroblasts. Rheinwatd and Green (1975), were the first to culture keratinocytes, shortly after which in (1977), they developed cultured epithelial autografts (CEAs) to treat partial thickness burns victims, with indefinite self-renewal (O'Connor *et al.*, 1981, Gallico III *et al.*, 1984).

To culture skin, *in vitro,* scientists have constructed an air-liquid-interface (ALI) (Pruniéras *et al.*, 1983). ALI overcomes incomplete differentiation associated with traditional culturing through the construction of a physiologically-appropriate setting. This is where the epidermal layer is exposed, superficially, to air and the dermal layer is allowed to interact with nutrients and liquid. The vital role of oxygen in skin tissue regeneration has been long known (Tammi *et al.*, 1979) and without which, ECM deposition will not occur (Kolesky *et al.*, 2014). This ALI has been used in conjunction with bioprinting to recreate bilayered skin constructs (Michael *et al.*, 2013, Lee *et al.*, 2009).

1.4 Bioprinting

The dynamic nature of medical research has shifted to embrace 3D printing. 3D printing or AM was developed in the early 1980's by Charles "Chuck" Hull, who out of intolerance, invented a fast-tracked design and production process (Kietzmann *et al.*, 2015). Chuck established a software interface capable of connecting a computer-aided design (CAD) with a 3D printer, STereoLithography (SLA), from which the Standard Tessellation Language (STL) file format arose (Grimm, 2004). The hardware process of SLA involves dispensing a thin layer of UV - curable liquid resin onto a platform. A concentrated beam of ultraviolet light "draws" a precise pattern which instantly solidifies. This process continues as the platform descends, adding layer upon layer of material, thus creating a 3D structure (Hull, 1986).

AM differs from traditional manufacturing techniques in that, as the name suggests, adds material instead of removing it. Previously, manufacturing has involved a top-down approach, where an excess of material is 'subtracted' or 'formed' into a final product (Mattox, 2013). Excessive amounts of waste are inevitable; nonetheless, the speed and scalability of this well-established method justify it's continued commercial use (Diegel *et al.*, 2010). AM, on the other hand, employs a bottom-up design approach. This process allows for a higher degree of customization and speed, appropriately coined rapid prototyping (RP). RP is significantly more sustainable; arguably one of the reasons it has become a favoured prototyping method by many companies such as Dyson™ (Gibson *et al.*, 2010). The ambition of AM is to have the technology available to everyone, to have the hardware in all households as if it were another inkjet or laser printer.

The scientific community, in particular, has come to incorporate AM into tissue engineering (TE) and regenerative medicine. In the early nineties, Langer and Vacanti (1993) pioneered TE as seeding isolated cells onto scaffolds. This results in non-specific scaffold geometry, porosity and cell placement. Many of the complexities involved in TE, or more specifically tissue regeneration, may be overcome through the utilisation of AM. Conventional AM techniques start with the generation of intricate 3D models through CAD. These are then translated into the STL file type mediating the computer and printer interaction (Mondy *et al.*, 2009). In bioprinting, the 3D models can also be generated from medical scans such as computed tomography (CT), magnetic resonance imaging (MRI) or X-rays, facilitating the onset of personalised medicine (Arai *et al.*, 2011, Keriquel *et al.*, 2010).

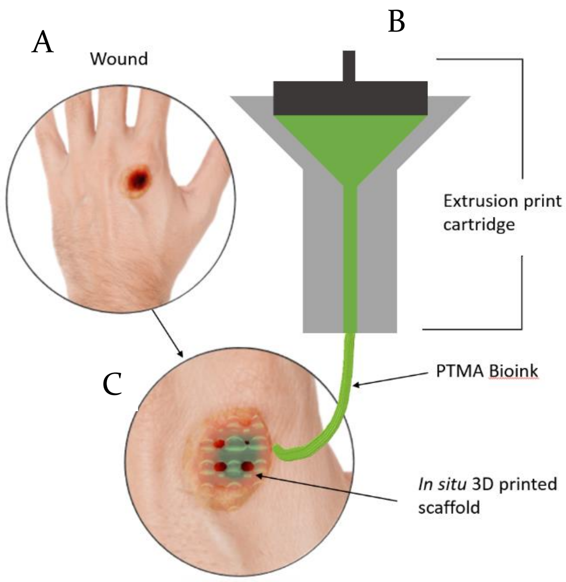

Figure 3 | A basic representation of an *in situ* skin bioprinting process. (A) Shows an image of a wound, (B) basic schematic of pneumatic print head and (C) shows *in-situ*/*in-vivo* extrusion bioprinting of a bioink scaffold.

As previously outlined, wound healing is an intricate process involving diverse cellular interactions. Bioprinting has given researchers a reliable means of replicating ECM and ECM components (Bártolo *et al.*, 2011), which could be used in developing wound healing models (Wigger-Alberti *et al.*, 2009). Patient-specific wound dressings or skin grafts could be fabricated with embedded ECM components, growth factors and cell types, precisely tailored to each region and wound depth, facilitating the body's natural response to trauma while protecting the site (Figure 3). The techniques available for such treatments are discussed in the next section.

1.4.1.1 Inkjet Printing

Inkjet printing technology can be split into continuous inkjet (CIJ) and drop-on-demand (DOD) printing. In the context of biofabrication, both CIJ and DOD inkjet bioprinting have, more suitably, been placed under the superficial umbrella of droplet-based bioprinting (DBB). Of which, DBB can be broken down again into three general branches, micro-valve, acoustic and inkjet bioprinting. For simplicity, only the thermal and acoustic or piezoelectric approaches will be discussed further if the reader wants intricate details regarding bioprinting mechanisms and techniques they are directed to reviews by Malda *et al.* (2013) and Murphy and Atala (2014).

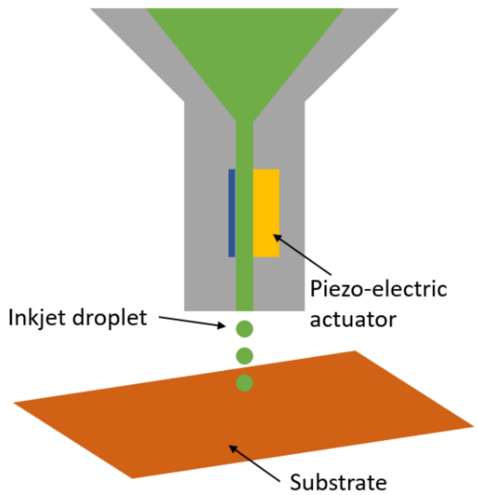

Figure 4 | A basic schematic of inkjet bioprinting. For simplicity, only the piezo-electric mechanism has been shown, generating high resolution droplet-based printing without the use of heating. Adapted from (Derby, 2010).

Thermal DOD bioprinting involves a micro-heater that vapourises the bioink shaping droplets through a pressure pulse (Derby, 2008). Piezoelectric DOD bioprinting forms droplets through mechanical actuation, without heating (Figure 4). Droplets are generated when a voltage is applied to a piezoelectric material, producing a pressure gradient, extruding the material (Tekin *et al.*, 2008).

As with all the bioprinting approaches, inkjet printing has its advantages and shortcomings. Regarding thermal approaches, inks are exposed to temperatures over 200 °C for short bursts. This is heavily reliant on the capacity of inks to recovery from abrupt temperature change, vapourising solvents. Interestingly, the impact on encapsulated cells seems to be negligible (Cui *et al.*, 2012, Xu *et al.*, 2006). Another significant shortcoming of these methods relates to the mechanical stresses imposed upon encapsulated cells, with a considerably narrow viscosity tolerance range (Figure 5)(Calvert, 2001). Moreover, frequent nozzle clogging and inconsistent droplet formation impart further difficulties. Typically, inkjet cartridges can fail once 400 000 cells have been printed (Parzel *et al.*, 2009).

Despite these limitations, however, printing resolution can be high, enabling precise control over bioink placement and consequently, the positioning of cells, below 100 picolitres (Calvert, 2007). Additionally, as mentioned, the availability and accessibility of such printers are vast, generally resulting in low maintenance and service costs.

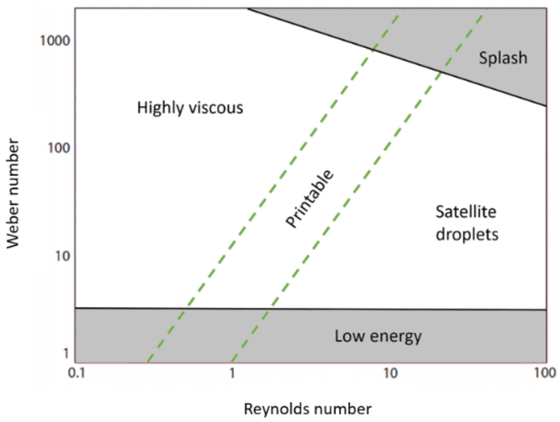

Figure 5 | Fluid properties where drop-on-demand inkject printing is feasible. Where the low energy area hinders dispensation and splash area results in uncontrolled ink placement. Adapted from (Derby, 2010).

1.4.1.2 Laser-Assisted Printing

Laser-assisted bioprinting (LAB) is based on laser direct writing and laser-induced forward transfer (LIFT) (Bohandy *et al.*, 1986, Koch *et al.*, 2010). Unlike inkjet printing, LAB does not require a printing nozzle, subjugating particular limitations. Figure 6 illustrates a simple representation of the technology, where a donor layer, containing an energy absorbing layer commonly made of gold or titanium but also polymers such as gelatin or triazine, are excited through laser pulses (Schiele *et al.*, 2010b, Schiele *et al.*, 2010a). These pulses penetrate and vapourise the donor layer, creating a bioink bubble. The formed hydrogel jet cascades onto the collector slide as a fine resolution droplet with high spatial control (Unger *et al.*, 2011). Droplet size can be regulated by laser energy, hydrogel depth and viscosity (Gruene *et al.*, 2011). The ink viscosity ranges for LAB methods are not as narrow as inkjet methods, 1 – 300 mPa.s^{-1} compared to 3.5 – 12 mPa.s^{-1} (Koch *et al.*, 2010). Correspondingly, as mentioned, nozzle, needle or tip clogging is not an issue.

LAB has been previously used in skin bioprinting (Koch *et al.*, 2010). With *in vivo* mice tests showing printed skin integrating with native host tissues (Michael *et al.*, 2013).

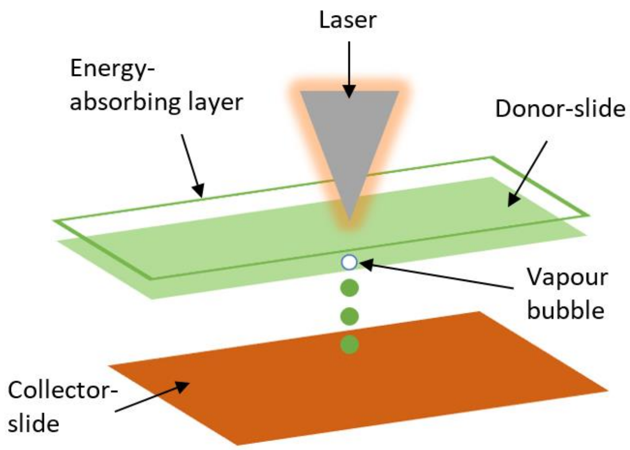

Figure 6 | Basic schematic of a laser bioprinter where a laser penetrates the absorbing layer vaporising the donor-slide creating a bubble dispensing a bio-ink droplet onto the substrate.

1.4.1.3 Extrusion Printing

Arguably the most extensively explored bioprinting approach in tissue engineering, used throughout this work, involves extrusion or micro-extrusion (Melchels *et al.*, 2014, Derby, 2012, Ferris *et al.*, 2013). Instead of droplets, extrusion-based techniques dispense continuous cylindrical strands of hydrogel through the air (Khalil and Sun, 2007) or mechanical force (Figure 7) (Jakab *et al.*, 2006). The former system employs pneumatics to drive the filament through the tip, restricted only by pressure and the delay of its volume. Mechanical or robotic extrusion printers use either piston or screw mechanisms to project hydrogels, with modest spatial control and resolution.

Due to simplicity, ink properties are not as restricted in this approach, supporting a vast viscosity range of 30 mPa/s to at least 6×10^7 mPa/s (Murphy and Atala, 2014). Moreover, extrusion techniques don't rely on focused heating. Recently, these systems have been developed to support multi-material printing, for further versatility (Kolesky *et al.*, 2014, Cathal *et al.*, 2016, Davoodi *et al.*, 2015).

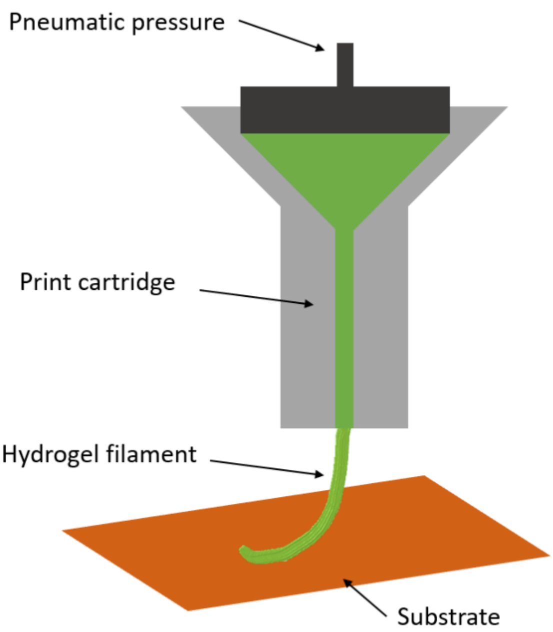

Figure 7 | General illustration of the pneumatic extrusion bioprinting technique.. For simplicity only pneumatic (air pressure) was drawn, two alternative mechanical methods exist, one utilising a piston and the other using a screw-based method.

The printer primarily used in this work was the 3D-Bioplotter™ (EnvisionTec, Gladbeck, Germany). The Bioplotter utilises pneumatic extrusion to dispense viscous hydrogels. The temperature controlled reservoir moves independently through X, Y and Z dimensions, placing materials onto a stationary temperature controlled substrate. Introducing the possibility of the use of thermosensitive inks for excellent control over material flow, attractive for cell encapsulation (Billiet *et al.*, 2012a).

A significant shortcoming of extrusion-based bioprinting, apart from the relatively average resolution, involves the shear stresses experienced by encapsulated cells during printing. Several approaches have sort to overcome this limitation. Hockaday *et al.* (2012) discussed the use of ultraviolet (UV) bioextrusion printing of PEG hydrogels. They found that the extrusion of cell encapsulated, low viscosity inks, capable of *in situ* crosslinking once extruded, would significantly reduce shear stresses on cells. Additionally, due to the post-printing chemical crosslinking by UV light, the resulting hydrogel had increased mechanical properties suitable for the regeneration of human heart valves. Further, Skardal *et al.* (2012), showed that the use of amniotic fluid-derived stem (AFS) cells in bioprinting could be a useful treatment for wounds and burns. They explored the use of AFS cells as they have high proliferation rates, favourable immunomodulating activities and tend not to form teratomas in mice (De Coppi *et al.*, 2007, Moorefield *et al.*, 2011). Thus, through the development of a suitable hydrogel, they were able to show AFS cells secreting growth factors at higher concentrations than mesenchymal stem cells (MSCs). Consequently, revealing the potential in exploring the use of new biomaterial-based hydrogels for bioprinting applications.

1.5 Hydrogels in Bioprinting

1.5.1 Structure

Hydrogels are three-dimensional hydrophilic polymer networks swollen in water. They are favourable materials for regenerative medicine due to their hydrophilicity, permeability, biocompatibility and dynamic compositional and structural similarities to native human tissues (Lee and Mooney, 2001, Gong *et al.*, 2003, Sun *et al.*, 2012, Gehrke *et al.*, 1997). These macromolecular networks can be composed of synthetic polymers such as poly(ethylene oxide) and Lutrol F127, or natural polymers such as gelatin, alginate, collagen, fibrin, and hyaluronic acid. The development of such hydrogel systems makes them valuable vessels for biofabrication (Nakamura *et al.*, 2010, Malda *et al.*, 2013, Billiet *et al.*, 2012b, Zorlutuna *et al.*, 2013).

The capacity of hydrogels to swell in water has been simplified into two mechanisms, '*bound water*' and '*free water*' (Hoffman, 2012). The former involves the interaction of polar-hydrophilic groups with water, followed by the binding of hydrophobic groups. Once swollen, the '*free water*' occupies space between polymer chains. Crosslinking and shear stress significantly influences this water absorbent capacity of hydrogels, pertinent to bioprinting (Figure 8) (Brannon-Peppas and Peppas, 1991, Pasqui *et al.*, 2012).

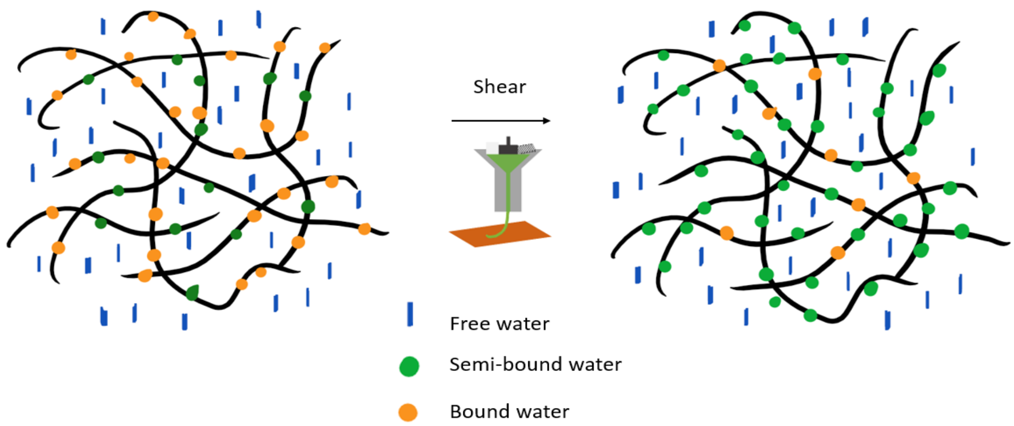

Figure 8 | Schematic representation of a swollen polysaccharide-based hydrogel on a macro-molecular scale. The left shows the native state with more bound water in the network with the right demonstrating a reduction in bound water due shear stresses imposed by bioprinting. Adapted from (Pasqui *et al.*, 2012).

Hydrogel properties can be engineered toward their final goal through the manipulation of polymer concentration and composition, along with crosslinking density and mechanisms. The crosslinking of polymer networks is undertaken by physical and/or chemical means, where appropriate physical gels can be formed via complexation, chain aggregation, hydrophobic association, hydrogen bonding, etc. (Hoffman, 2012, Ratner *et al.*, 2004, Berger *et al.*, 2004). Chemical crosslinking can be initiated via various mechanisms, including but not limited to enzymatic, redox-mediated, functional group reactions and free-radical photopolymerisation (Morelli *et al.*, 2015, Yang *et al.*, 2012, Shantha and Harding, 2002, Bertassoni *et al.*, 2014).

A recent emergence in composite and hybrid gels has seen significant improvements in physicochemical and mechanical properties. In particular, hydrogel mechanical properties can be engineered for specific applications; from cartilage regeneration and controlled release of biomolecules (Lin and Anseth, 2009) to bioengineering skin (Metcalfe and Ferguson, 2007a). One particularly interesting hybrid hydrogel recently came from the Massachusetts Institute of Technology (MIT), where researchers coated hydrogels with elastomers, preventing moisture loss while significantly enhancing hydrogel strength and flexibility (Yuk *et al.*, 2016). The researchers were then able to incorporate channels into the hybrid to mimic blood vessels which, when developed into a smart bandage, could be capable of monitoring skin physiology or in drug delivery.

Another noteworthy advancement in hydrogel development has come through the generation of interpenetrating polymer network (IPN) hydrogels, which are formed by interlacing two or more polymer networks on a molecular level. Additionally, robust gels have been made through double networks (DN) and ionic-covalent entanglement (ICE) gels (Sun *et al.*, 2012, Bakarich *et al.*, 2012). These hybrid and composite hydrogels have enabled researchers the means to overcome the innately weak mechanical properties most commonly seen in hydrogels (Sun *et al.*, 2012). However, some of these crosslinking mechanisms or agents produce cytotoxic by-products, impeding cytocompatibility and may not be suitable in bioprinting (Liang *et al.*, 2004).

1.5.2 Bioink and Printability

Biofabrication is a multidisciplinary research field which incorporates several aspects of science including physics, chemistry and biology with engineering. One particular component relevant to the field is rheology, which is found within the branch of physics and physical chemistry. Rheology characterises the flow and deformation of materials (Mezger, 2006). This characterisation technique is often overlooked in the context of bioprinting and can be broadly translated into the impact of printing constraints on bioinks (Malda *et al.*, 2013, Oyen, 2014).

'Printability' refers to an inks behaviour during and following extrusion. For instance, for ink to flow through a fine gauge needle, it should demonstrate shear-thinning behaviour and rapid recovery, or cessation, once placed onto the substrate (Jungst *et al.*, 2016). Ink viscosity determines printability, influenced by polymer concentration and crosslinking. Coupled with these material properties are the hardware restrictions bestowed upon inks, ranging from but not restricted to pressure, flow rate, temperature and substrate interactions (Murphy and Atala, 2014, Nikkhah *et al.*, 2012).

The printability of hydrogels is affected by crosslinking. Free-radical photo-polymerisation or crosslinking is a commonly used technique in biofabrication due to speed, simplicity and ability to be used *in-situ* (Malda *et al.*, 2013). The mechanism involves the generation of free radicals upon UV irradiation in the presence of a photoinitiator, producing covalent bond pairs (Petersen, 2012, Lü *et al.*, 2010). In doing so, particularly in hydrogels, this induces an increase in modulus, creating a stable, insoluble chemical network. Hydrogels are versatile materials that have the capacity to be chemically modified or functionalised with photo-polymerisable or crosslinkable groups (Geckil *et al.*, 2010, Kloxin *et al.*, 2009). For instance, carrageenan (Mihaila *et al.*, 2013), hyaluronic acid (Bencherif *et al.*, 2008) and gellan gum (Coutinho *et al.*, 2010) have all been functionalised to varying degrees with methacrylol moieties, to produce more physiologically stable hydrogels by light.

High viscosity results in high shear stress. A study recently published by Blaeser *et al.* (2015), discovered that high shear stress could result in damage to bioink encapsulated cells. Cells can thrive in appropriate culture conditions; thus a biofabrication window exists where there's a balance between hydrogel shape fidelity and favourable cellular conditions (Khalil and Sun, 2009, Malda *et al.*, 2013). Hydrogels as bioinks or as biopaper allow for the spatial separation of these encapsulated or seeded cells (Shariati and Moeinzadeh, 2015).

The hydrogels used have to be applicable to both the printing technique and the final application, from softer tissues such as cartilage (Markstedt *et al.*, 2015) and skin (Ringeisen *et al.*, 2004), to bone (Dash *et al.*, 2014, Hutmacher, 2000, Keriquel *et al.*, 2010). A potential source of these biomaterials is outlined in the next section.

1.5.3 Marine Polymers

It has been estimated that algae and phytoplankton contribute up to 50 % of the oxygen in the earth's atmosphere (Falkowski *et al.*, 1998, Qin *et al.*, 2012). The naturally derived polysaccharides from within these algae are abundant, sustainable, relatively cheap, resilient, and adaptable to suit a variety of medical applications (Andreakis and Schaffelke, 2012, Manivasagan and Oh, 2016). When compared to mammalian-derived polysaccharides (such as hyaluronic acid), algae tend to be natively biocompatible (Stevens, 2008). Thus these biomaterials are suitable ECM mimics, with the potential to be chemically modified for specific applications (Reys *et al.*, 2016, Rowley *et al.*, 1999).

One of the most studied polysaccharides from the algal origin is alginate, found in the cell wall of brown algae, primarily used as a thickening agent and in modern wound dressings (Straccia *et al.*, 2015). Over the years alginate has been shown to be useful in a variety of biomedical applications. In particular, an alginate-based hydrogel with an integrated unicellular green algae, *Chlamydomonas reinhardtii,* showed continual cell growth, proving that oxygen can be supplied or diffused into bioprinted constructs (Lode *et al.*, 2015). Alginate itself tends to lack cell adhesion molecules; thus collagen has been shown to increase cell adhesion and overall mechanical properties when added into a hydrogel system (Baniasadi and Minary-Jolandan, 2015). Huebsch *et al.* (2015) used an *in situ* injectable alginate-based hydrogels to regulate tissue repair, specifically, bone formation.

Agar and carrageenan, both extracts from red algae have vast biomedical uses. Interestingly, a three-year clinical cosmetic study showed that agarose, one fraction of agar, was a reliable filler used in lip augmentation, indicating greater biocompatibility than that of hyaluronic acid (Scarano *et al.*, 2009). Additionally, carrageenan has been combined with polyvinyl alcohol (a synthetic polymer) and agar in clinically tested hydrogels, for the treatment of wounds, burns and ulcers (Varshney, 2007).

A new type of algal polysaccharide, used in this work, is discussed in the next section.

1.5.3.1 Ulvan

Ulvan is a type of underutilised, anionic, sulphated polysaccharide with unique chemical and structural characteristics valuable for biofabrication (Chandika *et al.*, 2015). These characteristics, generally associated with attached sulphated rhamnose sugar include vast biological activity (Table 1). With such qualities, ulvan has great potential for a broad range of biomedical applications, including wound healing and the development of tissue-engineered skin grafts (Straccia *et al.*, 2015, Morelli and Chiellini, 2010).

Figure 9 | Image of different types of algae similar to that of which the ulvan polysaccharide is derived. Captured with a Leica d-lux typ 109 compact camera with 24 – 75 mm lens.

Table 1 | Biological actions of Chlorophytes (green macroalgae) and their polysaccharides, which ulvan can be extracted from.

Biological Activity	Reference(s)
Antiviral	(Damonte *et al.*, 2004, Cooper *et al.*, 2002)
Anti-inflammatory	(Toida *et al.*, 2003)
Antibacterial	(Straccia *et al.*, 2015, Kandhasamy and Arunachalam, 2008)
Anti-fungal	(de Freitas *et al.*, 2015)
Anticoagulant	(Costa *et al.*, 2010, Kanno, 2012)
Antioxidant	(Huang *et al.*, 2015, Costa *et al.*, 2010, Qi *et al.*, 2005)
Antitumour	(Kaeffer *et al.*, 1999)
Anti-proliferative	(Farias *et al.*, 2008)
Anti-thrombotic	(Lee *et al.*, 2004)
Anti-cholesterol	(Abe *et al.*, 2013)
Hypolipidemic	(Matloub *et al.*, 2015, Pengzhan *et al.*, 2003)
Immunomodulating	(Toida *et al.*, 2003).

The chemical composition of ulvan, comparable to other marine-derived polysaccharides, is complex and subject to seasonal variability (Johnson *et al.*, 1997, Abdel-Fattah and Edrees, 1973, Robic *et al.*, 2009c, Brading *et al.*, 1954). The two major disaccharide repeating units of ulvan (Figure 10) contain sulphate, xylose, rhamnose, glucuronic and iduronic acids resembling mammalian GAGs, namely, hyaluronic acid (HA), heparin, heparin sulfate (HS), iduronic acid in chondroitin sulphate (CS) and related GAG dermatan sulfate (DS) (Manivasagan and Oh, 2016). Unlike mammalian GAGs, plant-derived polysaccharides are inexpensive, sustainable and biocompatible.

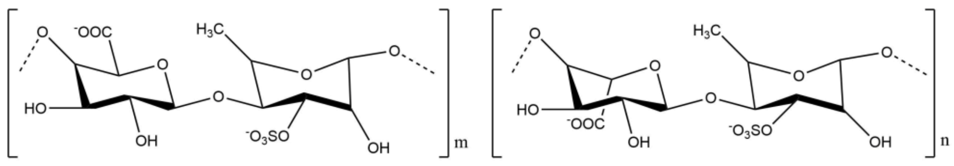

Figure 10 | The two main repeating units of ulvan. Note the presence of hydroxyl functional groups, the carboxyl group and the sulphate groups. Left Type A [→4)-β-d-Glcp-(1→4)-α-l-Rhap3S-(1→]n; right Type B [→4)-α-l-Idop-(1→4)-α-l-Rhap3S-(1→]n, created in Chemdraw®, adapted from (Jiao *et al.*, 2011).

The heparin-like structure of ulvan is thought to be a favourable characteristic for biomedical applications. Both heparin and HS are known to have considerable protein interactions, from influences on cell growth and differentiation, to interactions with morphogens, ECM components, and pathogens (Rapraeger, 1993, Bernfield *et al.*, 1999). One such protein interaction is utilised clinically; heparin is used as an anticoagulant due to its antithrombin-binding affinity, suggesting ulvan could have beneficial attributes if developed into a wound dressing (Esko and Linhardt, 2009). Additionally, effective artificial skin was designed by Burke *et al.* (1981) with a chondroitin sulphate based dermal matrix, yet another structurally similar GAG to ulvan.

Recent *in vitro* analysis of ulvan has shown an ability to scavenge reactive oxygen species or free radicals along with protecting human skin fibroblasts from injury by hydrogen peroxide (Cai *et al.*, 2016). The degeneration of human skin involves the weakening of fibroblast attachment to the surrounding ECM from enzyme catalysis, among other physiological phenomena. One such process accelerates ageing through the production of reactive oxygen species and hydrogen peroxide (H_2O_2) generation by mitochondria (Sohal and Sohal, 1991). A new study by Bhadja *et al.* (2016), exploring the benefits of *Ulva prolifera,* showed H_2O_2 inhibition, revealing potential anti-aging capacity. Moreover, sulphated polysaccharides have demonstrated efficacy against kidney stone formation (Bhadja *et al.*, 2016).

1.6 Aims and objectives

The ultimate goal of this study was to establish the groundwork for the 3D printing of ulvan-based hydrogels for wound healing applications. Specifically, PhycoTrix™ (denoted as PT), a sulphated marine-derived polysaccharide, taken from the cell wall of a DNA barcoded green algal spp., was utilised through the course of this study.

The outline, aims and objectives of this work were to:

- Chemically functionalise and characterise PT methacrylate (PTMA), to varying degrees, to produce a light curable-physiologically stable hydrogel.
- Develop a printable PTMA ink, through the introduction of a physical network to amend the viscoelastic bioink properties.
- Investigate the flow properties of the bioink in the context of extrusion-based bioprinting, through dynamic oscillations, flow and recovery analysis, to quantify its overall viscoelastic behaviour.
- Assess the crosslinking kinetics through *in-situ* rheology.
- Quantify, through micro-indentation, the necessary photoinitiator concentration and light energy required to produce a suitable skin tissue mimic.
- Understand the water uptake capacity of PTMA hydrogels under the same conditions as the mentioned indentation mechanical tests.
- Characterise the strut diameter, pore size and distribution of 3D Bioplotted scaffolds at various pressures, speeds and temperatures through imaging analysis.
- Explore the cytocompatibility through the use of human adipose-derived stem cells and mouse L929 fibroblast cells as a proof-of-concept wound healing model.

2 MATERIALS AND METHODS

2.1 Materials

The crude PhycoTrix™ extract, a sulphated marine-derived polysaccharide (denoted as PT here) was kindly supplied by Venus Shell Systems (VSS). All chemicals used were analytical grade supplied by Sigma-Aldrich (Australia) Pty Ltd unless stated otherwise and were used as received.

2.2 PT Functionalisation

2.2.1 Methacrylation of PT

PT extract obtained from VSS contained at least 40 % salt. Prior to experimentation, the extract was purified via dialysis against deionised (DI) water to eliminate salts and other small molecular weight impurities. Two different molecular weight cut-off membranes (MWCO) were used, 12 – 14 kDa and 3.5 kDa, along with both 4 and 24-hour purification times. DI dialysis water was changed once during the 4-hour purification and three times during the 24-hour dialysis. Samples were frozen at - 20 °C for at least 6 hours and collected by lyophilisation over 48 hours.

PTMA was synthesised according to (Morelli and Chiellini, 2010, Wang *et al.*, 2003, Rouillard *et al.*, 2011), where an excess of methacrylic anhydride (MA) – with a range of 20, 10, 5 and 2.5 molar excess with respect to the repeating units of the polysaccharide (containing three reactive hydroxyl groups) – was added to a 5 % PT solution (DMF/water (v/v, 1/1)). 5M NaOH was used to facilitate the substitution of hydroxyl groups with methacrylate groups (Figure 11).

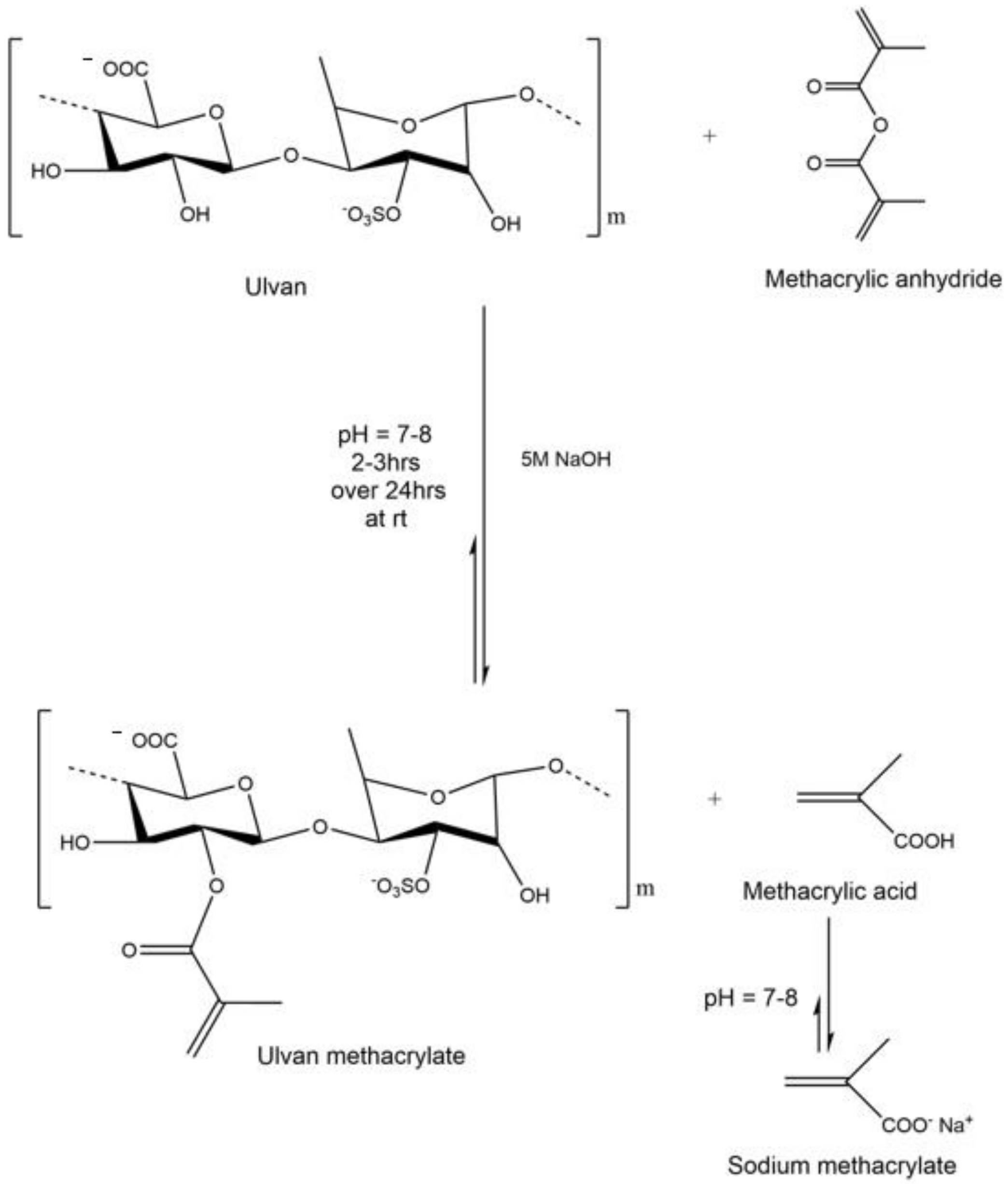

Figure 11 | General reaction scheme of PT functionalisation with methacrylic anhydride.

The reaction was tightly controlled under slightly basic conditions, with the pH being maintained between 7.5 and 8.5 to prevent basic ester hydrolysis, over 2 hours with vigorous stirring (Figure 12). The reaction was then left stirring at room temperature (~ 22 °C) for a further 22 hours. The reaction was then stopped with precipitation in 95 % ethanol (at least 5:1 v/v). The crude product was collected by centrifugation at 4400 rpm for 10 minutes, washed, then re-dissolved in DI water (made up to 5% solution of wet weight to reduce viscosity for dialysis). The solution was then dialysed (12- 14 kDa MWCO membrane) against DI water for 48 hours to remove remaining soluble unreacted anhydride and methacrylic acid by-products which could be cytotoxic. Samples were frozen overnight at - 20 °C and lyophilised for 72 hours. Dried samples were protected from light and stored at – 20 °C when not in use. The product was denoted as PTMAn, where n is 2.5, 5, 10, and 20 respectively.

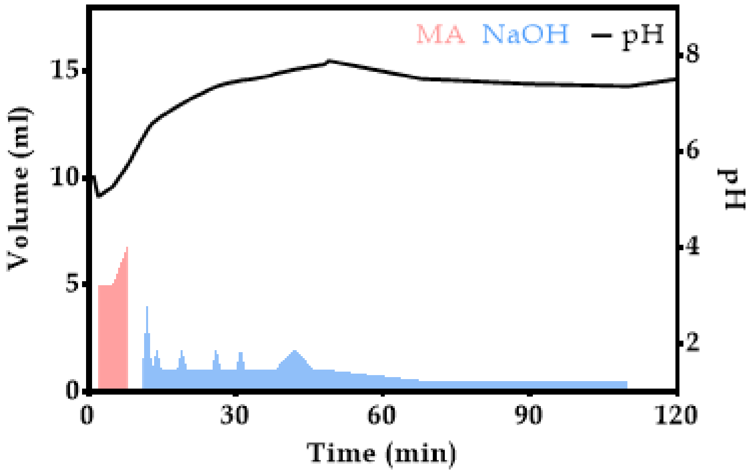

Figure 12 | Demonstration of PT functionalisation reaction with pH behaviour trend line in response to the addition of methacrylic anhydride (red) and sodium hydroxide (blue) over 2 hours. pH of the solution prior to the reaction ranged from 6.4 – 7 (of 5% sugar extract in water and organic co-solvent) then dropped to 5.3 – 5.6 with the addition of MA and once complete ranged from 7.2 – 7.7.

2.2.2 Fourier Transform - Infrared Spectroscopy

All infrared spectroscopic measurements were conducted on the IRPrestige-21 spectrometer (Shimadzu, Japan). To confirm esterification of PT, the freeze dried, functionalised extract was vacuum dried for 12 hours at 40°C to remove any residual moisture. Samples were analyssed in their solid state with a diamond attenuated total reflection (ATR) accessory, in the range 4 000 – 600 cm^{-1} at a resolution of 5 cm^{-1} after 32 scans. Atmospheric corrections were made when processing spectra in Shimadzu IRsolution software to eliminate moisture and carbon dioxide from the spectra along with Happ-Genzel apodisation, ATR correction, smoothing and baseline correction algorithms.

2.2.3 ^{1}H NMR Spectroscopy

To confirm purification and modification, proton NMR was completed comparing the crude, purified and modified samples. The system used was the Bruker AVANCE III 400, with the Bruker Ultrashield™ 400 PLUS magnet. Sample preparation included the use of 20 mg of freeze-dried sample dissolved in 0.6 ml of in deuterated water (D_2O). The analysis involved 1000 scans at 40 °C under water suppression to remove solvent peaks. Conditions: 6400 *Hz* spectral width, 2.6 s acquisition time.

2.2.4 Circular Dichroism

The Jasco J-810 spectropolarimeter was used for circular dichroism (CD) spectra analysis (180 – 210 nm). A 1 cm pathlength quartz cell was used with a scanning speed of 100 nm/min, response of 4 s, temperature 25 °C, with a three scan accumulation and bandwidth of 1 nm. Both samples purified PT and PTMA were prepared with 0.1 % freeze-dried polymer in DI water.

2.3 Ink Formulation and Characterisation

2.3.1 Ink Formulation

PT hydrogels were prepared as follows: 10 w/v% of PTMA10 was dissolved in DI water at 60 °C for at least 2 hours. Once dissolved, polymer solutions were then transferred directly into tinted printer cartridges. To this, 0.12 % (w/v) lithium phenyl-2,4,6-trimethylbenzoylphosphinate (LAP) photoinitiator was added along with 1 % of Penicillin-Streptomycin (P/S) and thoroughly mixed using a laboratory vortex mixer (JWA - Jencons Julabo Miximatic) at the highest speed for at least 1 minute at room temperature. Both 0.8 mM of boric acid and 0.25 mM calcium chloride, adjusted to a pH of ~ 7.5, were added and again vortexed for at least 2 minutes at room temperature. To remove air bubbles, cartridges were then centrifuged for 1 minute at 2200 rpm.

2.3.2 Rheological behaviour of PTMA ink

PTMA ink samples were prepared as above, without the P/S and LAP. The instrument used for the in-situ rheology was the Anton Paar - Physica MCR 301 controlled-stress rheometer (Anton Paar GmbH, Germany) outfitted with a 15 mm stainless steel parallel plate. All other measurements were conducted on the TA Instruments AR-G2 controlled-stress rheometer (New Castle, DE) using a 12 mm stainless steel parallel plate geometry, fitted with a Peltier temperature controlled stage. All samples were loaded in a liquid state. The geometry gap between plates was set to 500 μm for all tests with sample volumes of ~ 120 μL and ~ 80 μL for the MCR 301 and the AR-G2 respectively. Correct sample loading and trimming was crucial in ensuring reproducibility of results. All tests were completed in triplicate and subject to a constant 5-minute pre-shear of 5 s^{-1} to homogenise and retain shear history at required starting temperature (22 °C with the except of the temperature sweep which was set to 40 °C and ramped to 5 °C). A solvent trap was used with each run to reduce sample dehydration. Inks were all tested only once and discarded once investigated. The Lumen Dynamics Omnicure lx 400+ (400 nm light source) was mounted beneath the quartz plate on the MCR 301. Data analysis was initially conducted within the Rheology Advantage software by TA Instruments (TRIOS), finalised and presented with GraphPad Prism 6 (GraphPad Software, San Diego, USA). Parameters for each test are outlined in

Table 2.

Shear rate and Yield stress. A flow curve was determined by a continual ramp of shear rate from 0.01 to 10000 (s^{-1}) with time. To quantify the hydrogel's yield stress, an oscillatory stress ramp was conducted, where shear stress was increased from 0.1 to 1000 (Pa). Both tests were measured at 22 °C, 1 *Hz* frequency and 0.1 % strain.

Step-strain. Recovery of polymer network after an increase in strain from 0.1 % to 1000 % was assessed with a time sweep. The network was maintained at

0.1 % strain for 3 minutes then an abrupt increase in strain to 1000 % for 30 seconds, this was repeated 3 times investigate hydrogel recovery and imitate the extrusion-based bioprinting process. Measured at 22 °C for 21 minutes and 30 seconds, maintained at 1 *Hz*.

Table 2 | Dynamic oscillation rheology sweeps parameter summary.

Parameter	Temp-erature	Time	Strain	Frequency
Temperature (°C)	5 – 40 1.5/min	22	22	22
Equilibrium (min)	5	-	5	5
Gap size (μm)	500	500	500	500
Strain (%)	0.1	0.1	0.01 - 1000	0.1
Frequency (*Hz*)	1	1	1	0.1 - 20

2.4 Crosslinking kinetics by *in-situ* rheology

The photo-induced crosslinking kinetics of the PTMA ink was investigated by monitoring the real-time storage modulus upon exposure to UV irradiation (400 nm), through an *in-situ* rheology time sweep. This method was used to gauge the differences in polymer concentration along with photoinitiator and light energy needed to chemically crosslink PTMA hydrogels. The frequency was fixed to 10 *Hz* and strain to 0.1 %. All samples were exposed to light for 60 seconds while modulus was measured, measurements were taken for 60 seconds prior, during and following exposure.

2.5 Hydrogel Mechanics

PTMA inks were prepared as above (2.3.1) with the exception of photoinitiator concentration. Once the polymer solution was dissolved, LAP was added at final concentrations of 0.12 % and 0.06 %. Ionic gelation was achieved by the addition of 0.8 mM boric acid and 0.25 mM calcium chloride. To ensure homogenous gel formation samples were again vortexed for at least two minutes at the highest rate under ambient conditions.

Circular acrylic wells (10 mm diameter) were laser-cut and clipped on top of glass slides. Gels were heated to at least 40 °C or until they became liquid-like (for pipetting). 80 μL of each sample was then pipetted into each well and a glass coverslip clipped on top. All samples were exposed to 400 nm light for 60 seconds with varying light energies at room temperature (Figure 13). Immediately after curing, hydrogel constructs were removed and inundated with sterile deionised water to prevent dehydration.

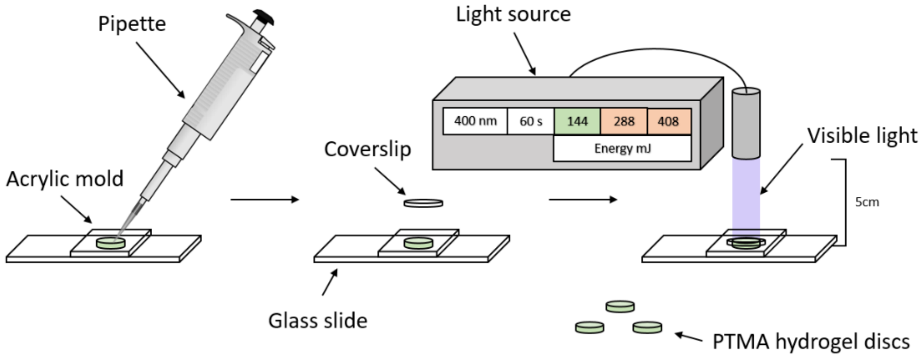

Figure 13 | Schematic of hydrogel well preparation, 80 µl of hydrogel was added into each well on a glass slide and a coverslip placed on top; each well was exposed to 400 nm light (Lumen Dynamics Omnicure lx 400+) at with varying energies for 60 seconds under ambient conditions.

Indentation. A micro-indentation test was used to determine the Young's modulus of photo-crosslinked hydrogels. A 10 N load cell was mounted onto the EZ-S mechanical tester (Shimadzu, Japan), an acrylate head with a flat tip of 0.990 mm diameter was used as the indenter to apply force to the surface of each hydrated hydrogel. Residual water used to prevent hydrogel dehydration was removed with a KimTech before testing. Trapezium X (Shimadzu, Japan) software compiled indentation data, which was then exported and presented with GraphPad Prism (GraphPad Software, San Diego, USA). To translate indentation depth, reduced modulus and applied force into Young's modulus we looked to Johnson (1985) and Naficy *et al.* (2013). Equation 1 was used to calculate the Young's modulus from the slope of the curve generated (stress as a function of strain) from the indentation readings. The reduced modulus (E*) was first calculated:

Equation 1 | Determination of Young's modulus through micro-indentation.

$$F = 2aE^{*}d \qquad (1)$$

$$(E^{*})^{-1} = (1 - v_1{}^2)E_1{}^{-1} + (1 - v_2{}^2)E_2{}^{-1} \qquad (2)$$

Where F is applied force, and d is indentation depth, collected through the indentation test and a was the indenter tip radius (0.495 mm). E_1 and E_2 are indenter and substrate moduli, and V_1 and V_2 are Poisson's ratios of both the indenter and substrate, respectively. It is assumed that the indenter is infinitely rigid thus reduced modulus (E*) can be removed and the equations can be simplified into (3), by substituting Poisson's ratio, where v_2 equals 0.5 (McKee *et al.*, 2011):

$$\boldsymbol{F = (\frac{8}{3})aE_2d} \qquad (3)$$

All experiments were performed in triplicate.

Water uptake. PTMA scaffolds were prepared the same way as indentation. Each construct was washed for 24 hours with DI water to remove any free polymer not covalently crosslinked. After being freeze-dried overnight (– 80 °C) each sample was weighed (W_i) and placed in DI water. Water was replaced regularly while samples were dabbed dry with a KimWipe to remove residual fluid and weighed at intervals of 3 hours, 6 hours, 9 hours and 24 hours (W_s). The WU was then calculated using equation 2.

Where W_s and W_i are weights of the hydrogels in their swollen and initial dry states, respectively. All experiments were performed in triplicate.

Error! Not a valid bookmark self-reference.

$$\boldsymbol{WU}\,[\%] = \frac{\boldsymbol{W_s - W_i}}{\boldsymbol{W_i}} \times \mathbf{100} \qquad (1)$$

2.6 Printing and Characterisation

Hydrogel bioprinting was performed on the 3D-Bioplotter™ (EnvisionTEC, Gladbeck, Germany) (FIG). The printer is stored within a biosafety cabinet to ensure sterility. All printing was conducted at room temperature ~ 22 °C with the substrate set to 16 °C, with the exception of strut diameter analysis (± 5 °C) (Appendix).

Scaffold Construction and Characterisation. 3D CAD through SolidWorks™ was employed to create the scaffold architecture. Initial cuboid scaffolds 10 x 10 mm were designed, exported as STL files and sliced within the Bioplotter RP® software. The infill of scaffolds set to angles of 0 ° and 90 °, with a print height of 0.112 mm in the Virtual Machines software (EnvisionTEC, Gladbeck, Germany). Once printed, the scaffolds were directly crosslinked with 400 nm light at 408 mJ for 120 seconds to ensure stability. Strut and pore architecture of printed constructs were assessed via optical microscopy (Leica M205A + Leica IC80 HD) along with the distance between pores (Figure 14).

EnvisionTEC 3D Bioplotter used for all printing throughout this work (A) and 3D Solidworks™ CAD model of 6-layer printed PTMA scaffold (B).

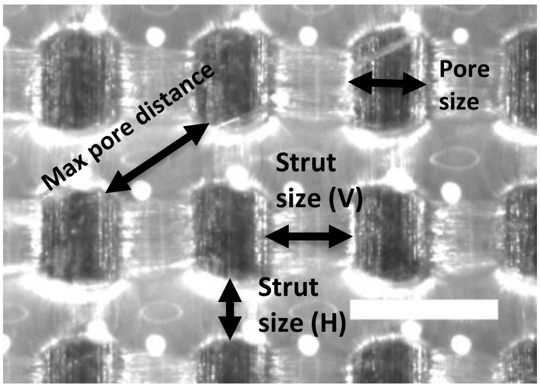

Figure 14 | Schematic showing scaffold architecture measurements of dual crosslinked PTMA hydrogel, of the strut (horizontal + vertical) and pore geometry, as well as max pore distance. ImageJ was used to enumerate distances, where n=5. Scale bar is 1000 µm. Printed at 2.5 bar and 9 mm/s.

2.7 Cytocompatibility

Initial cellular interactions and viability were assessed using L929 mouse fibroblasts (L929) and human adipose-derived stem cells (hASCs). 3D Bioplotted PTMA scaffolds were prepared using the same approach as outlined in 2.6, with the exception of 1 % penicillin-streptomycin (P/S) antibiotic. The printed scaffolds were washed with deionised water and freeze dried. The scaffolds were then UV sterilised for at least 30 minutes on each side.

L929 cells were cultured according to the standard procedures in high glucose Dulbecco's modified Eagle's medium (DMEM) supplemented with 10% fetal bovine serum in a humid incubator at 37 °C and 5% CO_2. hASCs were cultured in low glucose DMEM supplemented with 10% fetal bovine serum, 1% penicillin-streptomycin, 1% NEAA (non-essential amino acids) and 1 ng/mL β-FGF, at 37 °C/5% CO_2.

Cell seeding was conducted at a density of ~ 0.5 x 10^6 per scaffold. The viabilities of L929 and hASCs cultivated in the 3D printed scaffolds were monitored by fluorescence live/dead staining. The scaffolds were incubated with 5 μM calcein AM (for 30 min) and 10 $\mu g.mL^{-1}$ of propidium iodide (for 10 min) respectively in culture medium. Images of live (green) and dead (red) cells were then acquired by laser confocal fluorescence microscopy using a Leica confocal microscope (Leica TSC SP5 II).

3 RESULTS AND DISCUSSION

3.1 PT Purification

The crude salty PT extract, supplied by Venus Shell Systems Pty Ltd (VSS), was first purified by dialysis to remove excess small molecular weight impurities and potential contaminants from crude PT extract prior to functionalisation. Cellulose dialysis membranes with different molecular weight cut-off (MWCO), 3.5 kDa and 12 – 14 kDa, were employed respectively. Table 3 suggests no considerable difference between the two dialysis membranes during four-hour dialysis and longer dialysis time results in a greater removal of relatively low molecular weight PT fractions. In this work, a 24h-dialysis procedure was selected for purification of the crude PT extract obtained from VSS.

Table 3 | Purification yields of crude PT solutions by exhaustive dialysis against water with different MWCO membranes over 4 hours and 24 hours respectively at room temperature.

Dialysis membrane (MWCO)	Time (Hours)	Yield (%)
12-14 kDa	4	44
3.5 kDa	4	44
12-14 kDa	24	28
3.5 kDa	24	30

3.1.1 ¹H NMR

From the comparison of the ¹H NMR spectra from the crude and purified PT extracts we see the removal of sharp peaks at approximately 2 ppm, 3 ppm and 3.3 ppm (Figure 15), which were thought to be associated with low molecular weight impurities and fractions.

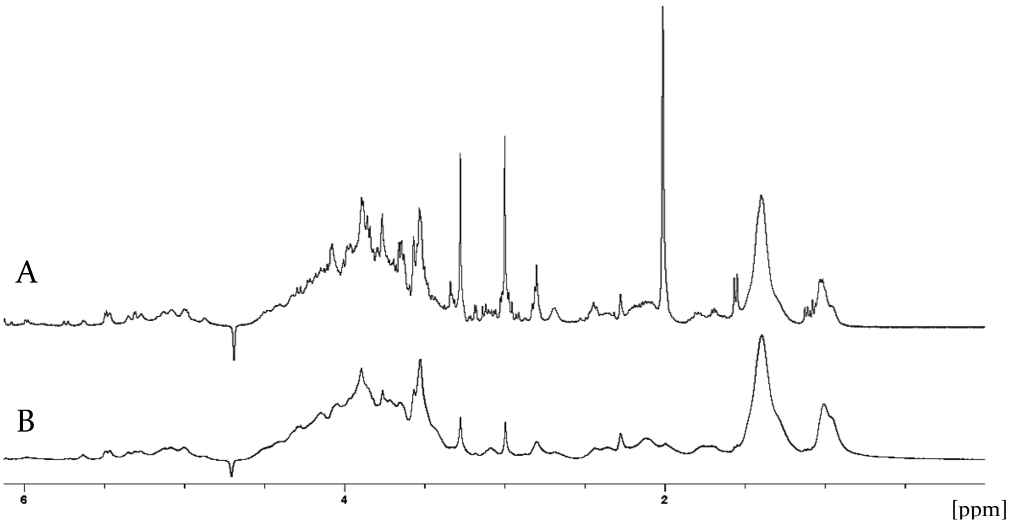

Figure 15 | ¹H NMR water suppression spectra of crude PT (A) and 12 – 14 kDa purified PT (B).

3.2 PT functionalisation and Characterisation

To be able to process PT for bioprinting it must be chemically modified due to its inherent aqueous solubility (Quemener *et al.*, 1997). To do this methacrylate functionalisation was employed. The two major repeating disaccharide units of PT contain three hydroxyl groups and one carboxyl group, all of which are sensitive to chemical substitution or functionalisation. Both methacrylic anhydride (MA) and butanediol diglycidyl ether (BDDE) have been shown to be successful in the chemical functionalisation of PT (Morelli and Chiellini, 2010, Alves *et al.*, 2013). A recent study of hyaluronic acid (HA) methacrylation suggested that the use of an organic co-solvent, DMF, could increase the degree of functionalisation (DoF) (Hachet *et al.*, 2012). Polymer methacrylation to varying degrees has previously been completed with gelatin (Hoch *et al.*, 2013), gellan gum (Coutinho *et al.*, 2010), fucoidan (Reys *et al.*, 2016) and carrageenan (Mihaila *et al.*, 2013).

3.2.1 Fourier Transform - Infrared Spectroscopy

The chemical characterisation of PT by Attenuated Total Reflectance Fourier Transform Infrared (ATR-FTIR) spectroscopy confirmed the presence of substituted methacryloyl groups onto the polymer backbone. Broad peaks between 3500 - 3200 cm^{-1} are characteristic of polymeric hydroxyl groups (Figure 16) (Alves *et al.*, 2013). The sharp peaks at 1640 cm^{-1} and 1050 cm^{-1} are associated with C-O stretches, consistent with previous studies (Morelli and Chiellini, 2010, Pengzhan *et al.*, 2003). Regular peaks between 700 - 1200 cm^{-1} are linked to the sulphate and rhamnose groups present in the polymer (Pengzhan *et al.*, 2003). The peak at ~ 1720 cm^{-1} in PTMA20 and PTMA10 to a less extent in PTMA5, not present in the native PT, correspond to the introduced carbonyl methacrylate group, consistent with previous work (Morelli and Chiellini, 2010). Interestingly, the peak was barely visible in the 2.5 molar excess reaction. Thus further analysis was undertaken with ^{1}H NMR spectroscopy.

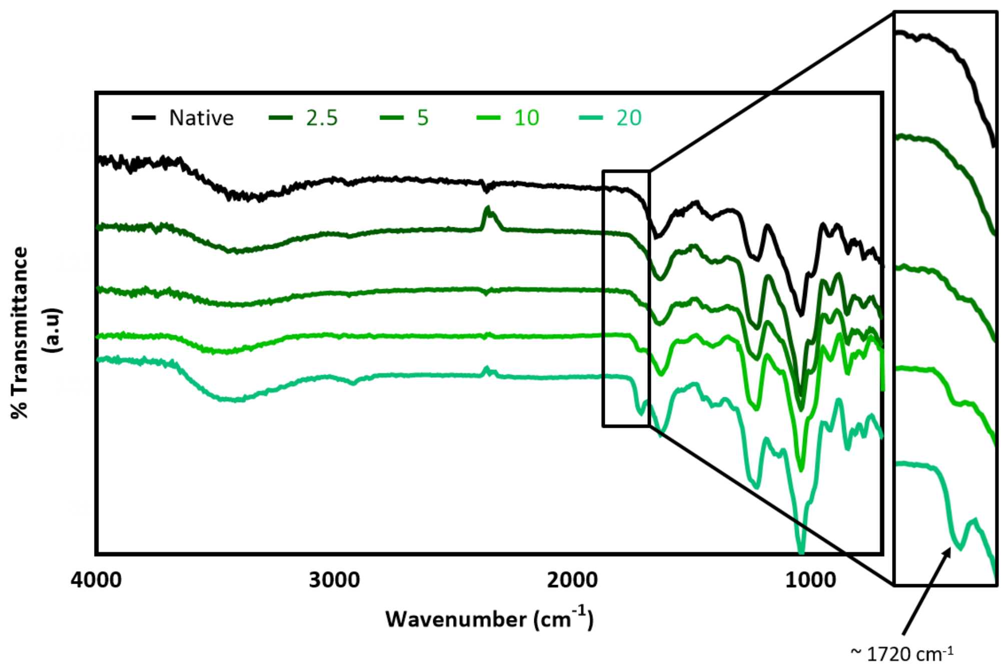

Figure 16 | ATR-FTIR spectra of native PT (top) and modified PTMA samples, from 2.5 to 20 molar excess reactions, showing a gradual increase of the peak at 1720 cm^{-1} indicating a higher degree of functionalisation with increasing anhydride.

3.2.2 ^{1}H NMR Spectroscopy

The degree of functionalisation (DoF) was determined by comparative analysis of the ^{1}H NMR spectra of purified PT with PT methacrylate (PTMA). The maximum DoF was three as native PT contains three hydroxyl groups per repeating unit. The successful substitution of MA groups was confirmed (Figure 17) where peaks at approximately 5.9 ppm and 6.3 ppm were present, typical of two protons linked to a vinyl group ($-C=CH_2$) (Chiellini and Morelli, 2011). Methyl protons of the native rhamnose are assigned in the region of 0.9 to 1.1 ppm. The peaks observed between 1.9 and 2.2 ppm represent the methyl protons next to the double bond from MA ($CH_3-C=CH_2$), not present in the unmodified PT sample.

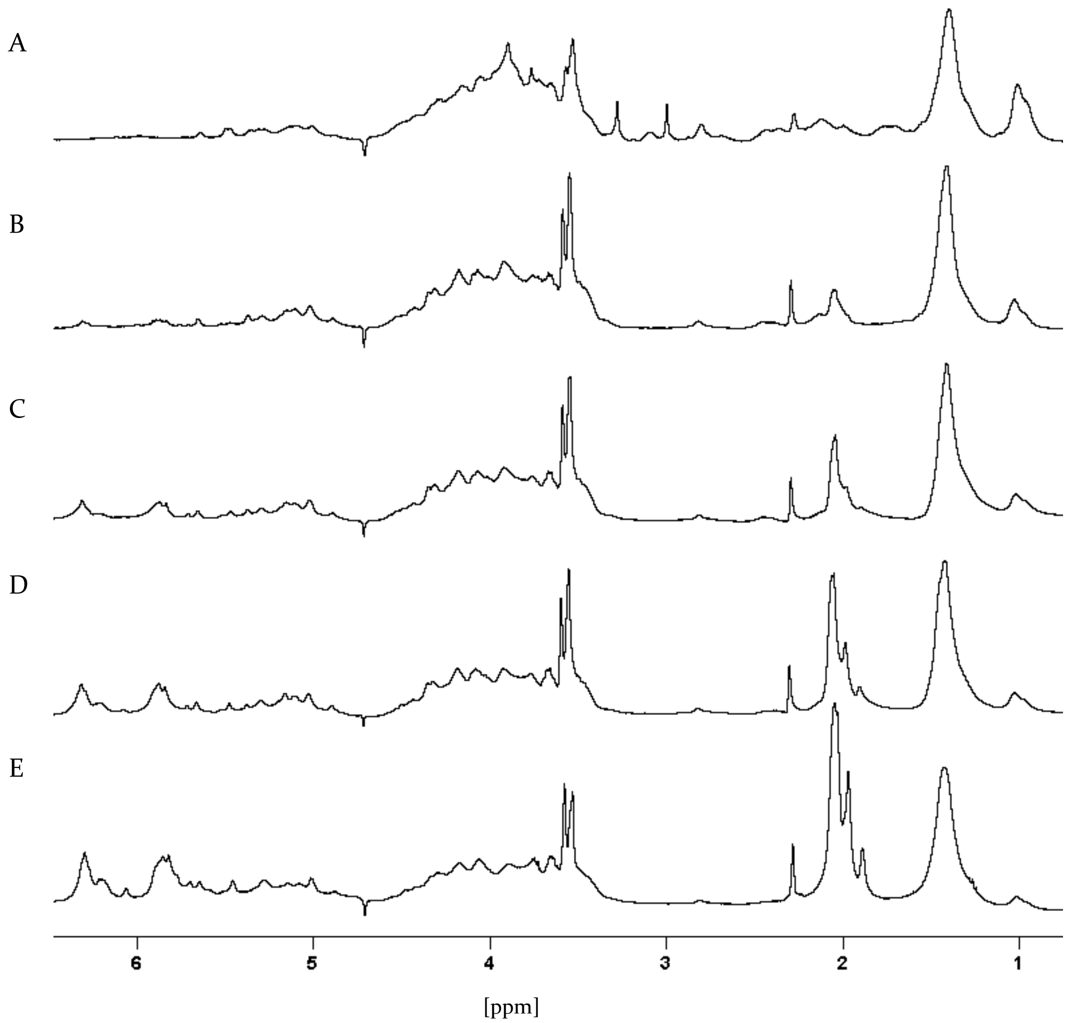

Figure 17 | ^{1}H NMR water suppression spectra of unmodified-purified PT (A), PTMA2.5 (B), PTMA5 (C), PTMA10 (D) and PTMA20 (E).

Broad peaks in the spectra could be due to retarded polymer chain mobility as a result of high molecular weight, characteristic of polymers and/or formation of microaggregates in aqueous solution, reported by related studies in ulvan (Lahaye and Robic, 2007, Robic *et al.*, 2009b, Ray and Lahaye, 1995).

Table 4 summarises the ^{1}H NMR findings. Relative DoF increased with the amount of methacrylic anhydride put into the reaction, consistent with previous studies including kappa-carrageenan, chondroitin sulphate and gellan gum modification (Reys *et al.*, 2016, Bryant *et al.*, 2004, Coutinho *et al.*, 2010, Mihaila *et al.*, 2013). Further, through the use of the organic co-solvent, the functionalisation efficiency appeared to increase when compared to previous PT functionalisation (Morelli and Chiellini, 2010).

Table 4 | The degree of functionalisation (DoF) from ^{1}H NMR analysis. Percentage yield was determined once collected by lyophilisation over 48 hours. Relative DoF was determined by comparing the integrated intensity of the double bond peak to that of the rhamnose methyl protons.

Reaction	DoF	Yield (%)
PTMA20	1.8	62
PTMA10	1.0	63
PTMA5	0.5	56
PTMA2.5	0.2	60

3.3 Ink Characterisation

3.3.1 Ink formulation – preparation of physically crosslinked PTMA

The introduction of methacrylate groups onto the PT polysaccharide backbone enables photo-triggered chemical crosslinking in the presence of a photoinitiator (LAP at 0.06 % and 0.12 % w/v). As ionic networks have been shown to be weak under physiological conditions due to the exchange of divalent cations by monovalent cations, a covalent network was introduced to ensure the stability of 3D printed structures (Coutinho *et al.*, 2010).

Required polymer concentration was first evaluated through *in situ* rheology (Figure 18). The crosslinking kinetics, to quantify light energy and photoinitiator concentration, were assessed independently by the same method in a subsequent section. An increase in storage modulus (*G'*) was observed with increased polymer concentration, independent of photoinitiator concentration. 5 % of PTMA10 saw a slow increase in *G'*, with an elongated 'lag phase', suggesting minor chemical network formation within the timeframe tested (60 seconds). Both 7 % and 9 % exhibited a more substantial *G'* increase, with the latter increasing approximately one order of magnitude compared to the ionic network. This is simply due to the presence of more methacrylate moieties available for photopolymerisation. Increasing the polymer concentration further (beyond ~ 10%) results in slight hydrophobicity and aggregation thought to be associated with the multitude of methyl groups attached to the rhamnose sugars (Cunha

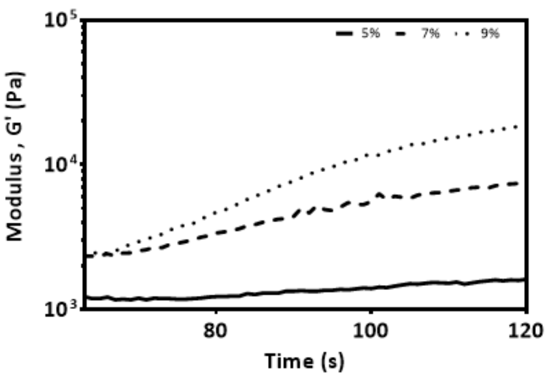

Figure 18 | *In-situ* rheology of 5 %, 7%, and 9 % PTMA10 demonstrating storage modulus (Pa) as a function of time (s) over a 60 second with 400 nm light exposure at 408 mJ. All samples contained the same photoinitiator concentration (0.12 % w/v).

and Grenha, 2016). Thus, all further testing was completed at 9 % to ensure sufficient chemical crosslinking with 60-second irradiation in the presence of a sufficient concentration of LAP.

PT has been shown to form an ionic network with boric acid and calcium chloride at a pH of ~ 7.5 (Haug, 1976, Lahaye and Axelos, 1993, Lahaye and Ray, 1996). In order to develop a suitable hydrogel for bioprinting, a qualitative tilt method was employed to assess the physical gelation at the set polymer concentration.

The highly substituted PTMA20 solution did not form a gel at the tested boric acid and calcium chloride concentrations (0.8 mM and 0.25 mM respectively) when compared to the native PT. Steric hindrance associated with the introduced functional groups required an increase in ion concentration to form a stable ionically crosslinked gel. Additionally, through the PTMA functionalisation, the number of free hydroxyls are reduced, obstructing the formation of borate ester-calcium stabilised "junction zones", a proposed mechanism for physical gel formation (Robic *et al.*, 2009a). Further, as outlined through CD analysis, the native PT's disordered molecular configuration could expose itself to a denser physical network formation; as the PTMA macromers most likely align with the introduced methacrylate groups (Appendix). A basic schematic of dual-network PT bioink development is outlined in Figure 19.

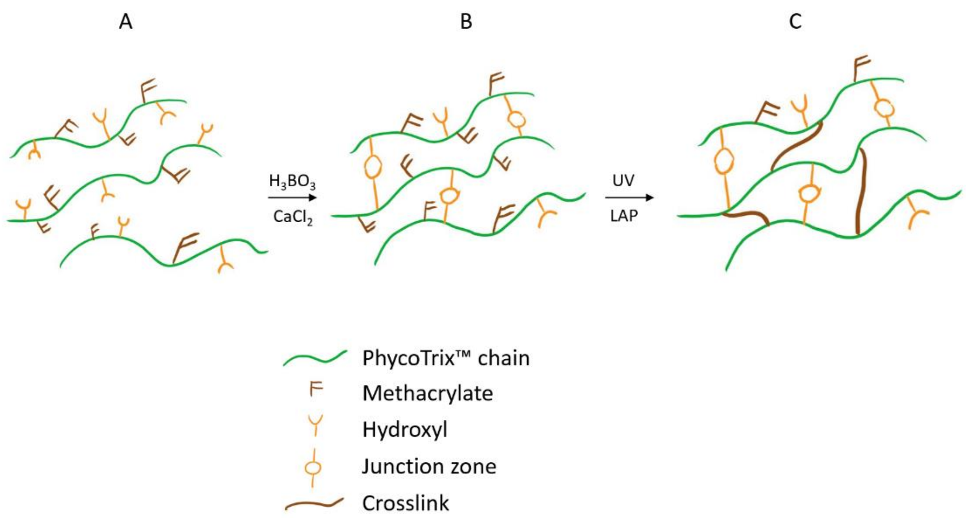

Figure 19 | Possible schematic representation of bioink development including the production of ionic and chemical polymer networks. Where A represents the modified PTMA solution, B is the ionically crosslinked PTMA with introduced boric acid-calcium ion stabilised ester linkages and C the production of chemical network through photo-crosslinking in the presence of LAP photoinitiator.

Once concentrations were justified, printability was evaluated through a syringe. The hydrogels had to have a viscosity that would allow flow through a 27 gauge needle (~ 150 μm) with adequate structure retention and enough resistance to deforming and flowing from the tip once extruded. A 9 % PTMA10 polymer concentration allowed for sufficient photopolymerisation as well as a reduction in boric acid concentration, shown to be toxic at high concentrations (McNally and Rust, 1928, Schillinger *et al.*, 1982). That said, boronic acid an alkyl substituted boric acid has previously been employed in hydrogel development (Konno and Ishihara, 2007). Specifically, a PVA/boronic acid hydrogel was used in fibroblast L929 cell encapsulation. Proliferation rates were consistent with that of the control, suggesting it was not detrimental to cells at low concentrations.

3.3.2 Rheological behaviour of the PTMA ink

A rheological evaluation was undertaken to assess, quantitatively, the printability of the physically crosslinked PTMA hydrogel ink. Small amplitude oscillatory shears (SAOS) were established to investigate the viscoelastic properties of hydrogels, within the linear region (sinusoidal). Rheology is paramount to understanding the fluidic behaviour of polymer-based hydrogels for bioprinting (Li *et al.*, 2016). For optimal printability, a hydrogel should demonstrate viscoelastic solid-like behaviour at low shear rates but yield and start to flow above a particular yield stress (Stokes, 2011).

3.3.2.1 Temperature and Time

For a hydrogel to be a viable bioink, it must be stable and printable within a cytocompatible temperature range, particularly if cells are encapsulated. To understand gelation temperature of the ionically crosslinked PTMA hydrogel, *G'* and *G"* were analysed while the temperature was ramped on a Peltier plate. Figure 20A, shows the temperature sweeps of PTMA with and without ionic crosslinking. The PTMA solution without ionic crosslinking exhibits liquid-like behaviour with much weaker moduli, rendering itself inadequate for use alone in extrusion printing. The ionically crosslinked gel behaves as a viscoelastic solid within the temperature range tested (5 – 40 °C), where the *G'* starts one order of magnitude higher than *G"*, signifying the presence of a resilient elastic network up to approximately room temperature (22 °C). The physically crosslinked PTMA hydrogel seems to have a broad temperature window in which it behaves as a viscoelastic solid, suitable for extrusion-based bioprinting techniques. This may also provide a facile approach using temperature to control and regulate the 3D printed structures based on PTMA.

In this project, due to time constraints, room temperature was selected for all the 3D printing studies undertaken. As such, all further rheological tests were conducted at 22 °C. That said, this highlights the advantage of the PTMA ink in practical applications, making it more applicable to a variety of printing hardware that do not have temperature controls.

A time sweep was conducted to establish the stability of the ionically crosslinked PTMA hydrogel at room temperature at a constant frequency and strain (Figure 20B).

Over the 20 minutes tested the gel showed no dramatic change in *G'* and *G"* suggesting consistency and stability under ambient conditions.

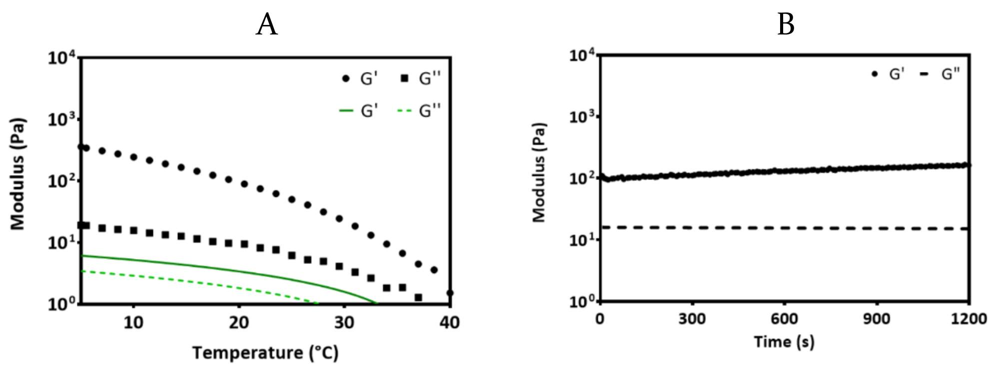

Figure 20 | (A) Temperature sweep from 5 – 40 °C showing storage (G') and loss (G") modulus as a function of temperature (°C) of ionically crosslinked hydrogel (black) and PTMA solution(green). (B) time sweep over 20 minutes showing storage (G') and loss (G") modulus as a function of time (s), at room temperature (~ 22 °C).

3.3.2.2 Amplitude and Frequency

A strain amplitude sweep (Figure 21A) between 0.1 % and 1000 % showed a relatively broad linear response in *G'* (the linear viscoelastic region or LVR) to increased strain up to ~ 90 %. Following this, a tightening effect on the polymer network, as indicated by an increase in *G'*, was noted when increasing the strain from ~ 90 % to ~ 150 %. The tightening could be associated with the reorganisation of the polymer network in PT (Robic *et al.*, 2009a). The hydrogel's network then undergoes deformation, or even collapse beyond ~ 150 % strain. This could be due to disruption of some intermolecular interactions including the ionic network interactions, as reported in alginate hydrogels (Webber and Shull, 2004).

Based on the strain amplitude sweep, a strain of 1 %, within the LVR range, was selected for the frequency sweep. A frequency range of 0.1 to 20 *Hz* was chosen as it covers some of the most common forms of regular human activities that impact the bodies external environment (Figure 21B) (Farley and Gonzalez, 1996, Gutmann *et al.*, 2006, Kokshenev, 2004, Danion *et al.*, 2003). The storage modulus of the ink was steady with only a slight linear increase up to 8 *Hz*, implying a solid-like structure. This is also supported by the phase angle (δ) data primarily existing beneath ~ 10 °. These frequency sweep results are consistent with ulvan/PVA solutions (Toskas *et al.*, 2011). Above 8 *Hz* however, phase angle begins to increase, indicating the onset of destabilisation of the polymer networks.

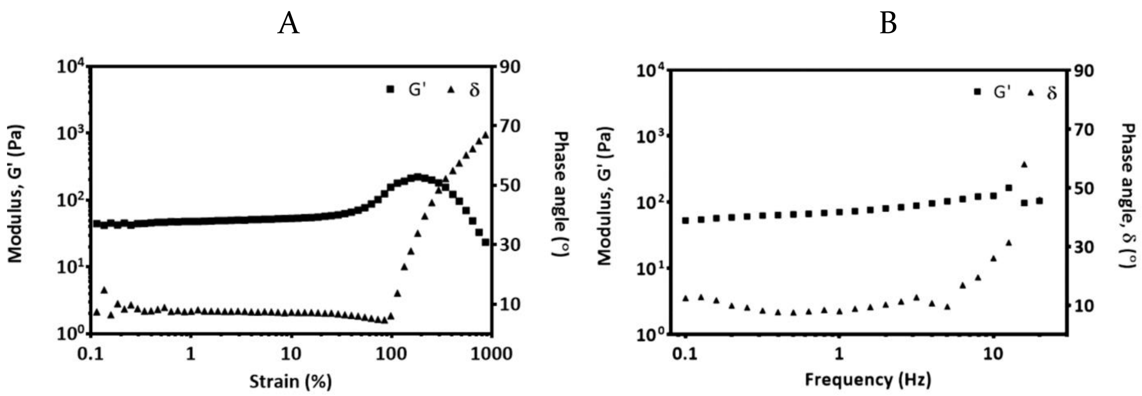

Figure 21 | (A) Strain sweep showing storage modulus (G') as a function of strain. (B) Frequency sweep showing storage modulus (G') and phase angle (°) as a function of frequency at room temperature (22 °C).

3.3.2.3 Flow and Yield Stress

For extrusion-based bioprinting, whether it be pneumatic or mechanical, high viscosity, shear thinning bio-ink is ideal, as it allows for the material to flow under pressure or with increased shear. Once pressure stops, ink viscosity should provide cessation. This not only enables the ink to retain its shape once extruded, but also allows it to be entrenched within the extrusion tip instead of dribbling out. Hydrogels with these attributes are ideal for bioprinting, reducing tip obstruction thus preserving consistency (Skardal *et al.*, 2010).

The viscosity of PTMA hydrogels is impacted greatly by polymer and ion concentration. Shao *et al.* (2014) showed a different species of ulvan to have a shear thickening behaviour in solutions with concentrations below 1 %. The thickening is attributed to the deformation ulvan ultrastructure and ultimately the disintegration of bead agglomeration, formerly recapitulated. This thickening behaviour was not observed at the high concentrations of PTMA hydrogels tested throughout this work.

Figure 22 shows both shear rate and yield stress rheological measurements. The ink's apparent viscosity exhibits a non-Newtonian fluidic and shear-thinning behaviour as the polymer networks align in response to applied shear stress (Figure 22A) (Hanson Shepherd *et al.*, 2011). This trend is consistent with studies from former Ulvaceae related rheology (Qiao *et al.*, 2016).

Once it was established that the hydrogel behaved as a shear-thinning, non-Newtonian viscoelastic fluid, formerly coined pseudoplastic, a yield point measurement was then conducted. The yield point is, in engineering terms, the stress at which deformations force the network from an elastic to a plastic state. Under this point, the material can return to its original state, beyond it, however, the material will undergo some irreversible deformation. The yield point was determined to be ~ 500 Pa where n=3. Upon a pneumatic pressure increase, the ionic polymer network progressively undergoes restructuring and realignment with long polymer units unravelling, flowing in the direction of least resistance and reaching a breakdown point of the polymer networks.

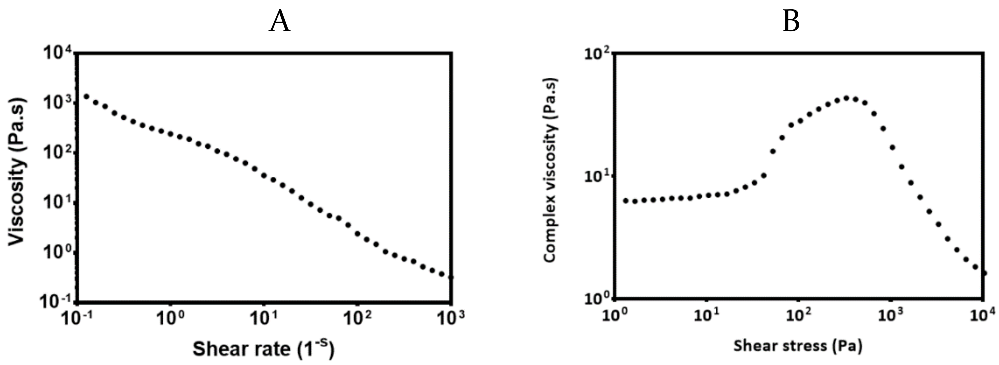

Figure 22 | (A) Flow profile showing viscosity (Pa.s) as a fucntion of shear rate. (B) Yield stress measurement showing complex viscosity (Pa.s), not static, as a function of shear stress. Both measurements were analysed at room temperature.

3.3.2.4 Step-strain

From the above amplitude sweep, yield stress and flow behaviour we can assess potential injectability or, more appropriately, the printability of formulated hydrogels. Furthermore, we have also examined the self-recovery capacity of the PTMA ink in the context of bioprinting, the key to achieving high fidelity printed structures.

To imitate the printing process a step strain measurement was conducted, where amplitude was maintained at 0.1 % for 3 minutes and abruptly increased to 1000 % for 30 seconds to deform the ionically crosslinked PTMA gel. 1000 % was used due to deformation of the polymer network observed in the strain amplitude sweep. This was repeated three times and the modulus response assessed (Figure 23A, B).

Upon pneumatic extrusion through a small gauge printing needle, shear stresses are dramatically increased, dependent on material viscosity and pressures used. As shown in Figure 23A, the ionically crosslinked polymer network seemed to recover and maintain a storage modulus following the first strain increase, between 460 and 350 Pa. This demonstrates a rapid recovery of hydrogel mechanical properties, allowing for retention of structural integrity for consistent curing, post printing. In the mean time, as with the viscosity viscosity study, a thixotropic behaviour was also demonstrated with a reduction in storage modulus during the increased strain (Michael *et al.*, 2015).

The PTMA ink demonstrated favourable printing behaviour including shear-thinning and rapid self-healing properties. This enables extrusion of filaments at low nozzle pressure, to protect cells from physical stress while then achieving high fidelity printed constructs.

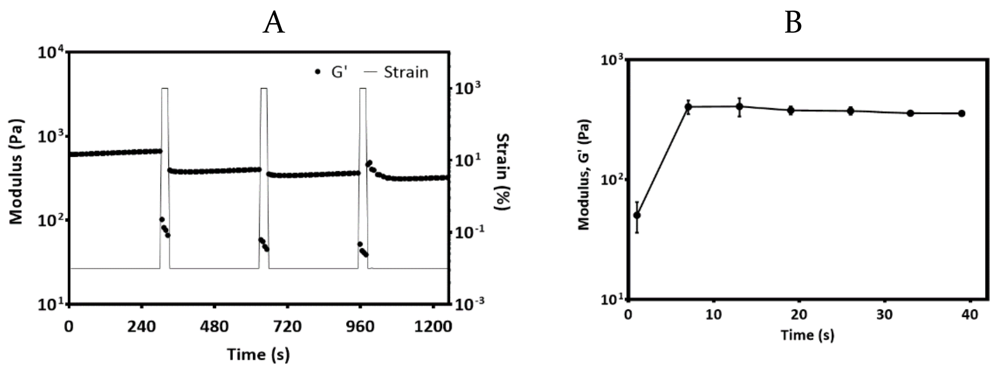

Figure 23 | (A) Step strain measurement at 22 °C. (B) Storage modulus recovery against normalised time in seconds, representing the general response average ± SD, where n=3.

3.4 Crosslinking kinetics by *in-situ* rheology

The crosslinking kinetics of PTMA inks were assessed by *in-situ* rheology. Samples containing either 0.06 % (w/v) and 0.12 % (w/v) LAP were tested over 180 seconds. The first 60 seconds were used for equilibrium, monitoring the storage modulus (*G'*) of the physically crosslinked networks. Irradiation with 400 nm light at three different light energies was initiated at the 60-second mark, exposed for a total of 60 seconds then turned off. *G'* was detected for a further 60 seconds following exposure to observe any changes.

The onset of photo-crosslinking was less efficient with reduced LAP (Figure 24A). A distinct lag period of approximately 15 seconds was observed in the sample containing 0.06 % (w/v) LAP and irradiated at 144 mJ. For the rest of samples, the lag phase was shorter, less than 10 seconds, which is attributable to increased LAP concentration and/or increased irradiation energy. Billiet *et al.* (2014) compared irradiation kinetics of the two photoinitiators, Irgacure 2959 and VA-086. Both of these initiators demonstrated a longer lag period compared to the LAP photoinitiator used throughout this work, with VA-086 being least efficient.

Figure 24 shows a marked increased in *G′* for all the samples upon photo-crosslinking. For instance, an increase of approximately one order of magnitude in *G′* was noted in the samples with 0.12% (w/v) LAP and exposed at a 408 mJ irradiation energy (Figure 24B). In addition, all samples appeared to reach a *G′* plateau following

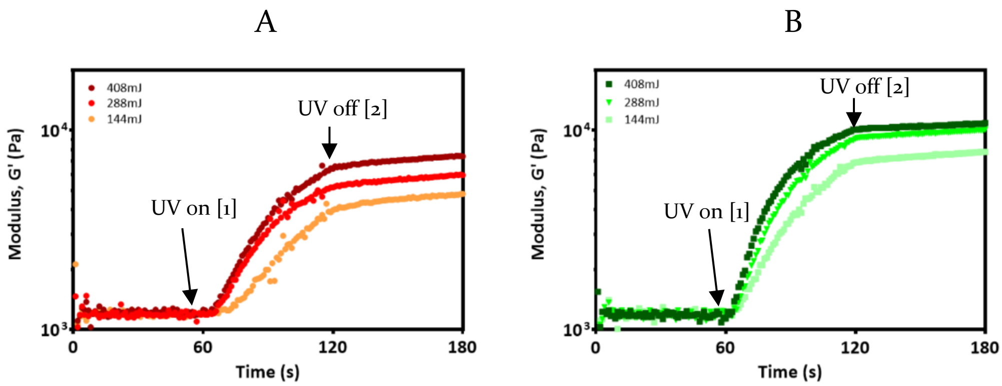

Figure 24 | In-situ rheology demonstrating the crosslinking kinetics of 9% PTMA hydrogels over time. (A) Shows low photoinitiator concentration (0.06 %) and (B) shows the high photoinitiator concentration (0.12 %). Where 1 and 2 indicate the start and stop of irradiation, respectively. All tests were completed at 22 °C.

60s irradiation, after which a slight increase in G' was noted for the following 60s. This suggests a near completion of photo-crosslinking at the end of the 60s irradiation, which is in direct contrast to the aforementioned study, showing G' continuing to increase significantly once curing was stopped.

The difference in photo-crosslinking kinetics could be due to several factors, for instance, the efficiency of free radical production by the different types of photoinitiators, irradiation energies, types of free radicals produced, polymer concentration and the amount of reactive groups available. To be suitable for biomedical applications, particularly bioprinting, minimal photo-initiator concentration, light exposure time and energy are ideal for minimising any adverse effects on cell viability and function.

3.5 Hydrogel Mechanics

Functionalisation of PT introduces photo-polymerisable groups onto the polysaccharide backbone. Once these reactive double bonds have been introduced an ionic network was introduced to increase viscosity for printability. Previously, Schuurman *et al.* (2013) outlined that parameters such as DoF, solvent, photoinitiator concentration, UV intensity and crosslinking temperature should remain constant as they can impact crosslinking kinetics within each system.

3.5.1 Indentation

Micro-indentation was performed on disc-like samples (10 mm diameter, 1.5 mm thick) to determine the Young's modulus of PTMA hydrogels (Figure 25– A, B). Two different LAP photoinitiator concentrations, along with three different irradiation energies at 400 nm were used. A gradual increase from 20 kPa to 40 kPa was observed in the samples crosslinked at the lower concentration of LAP (0.06 % (w/v)). Interestingly in both systems, there was no significant difference between the 288 mJ and 408 mJ light intensities, suggesting a threshold may have been reached in free radical generation. The samples prepared at a higher concentration of LAP (0.12 %(w/v)) showed a Young's modulus approaching that of the dermal human skin layer, approximately 75 kPa (Liang and Boppart, 2010).

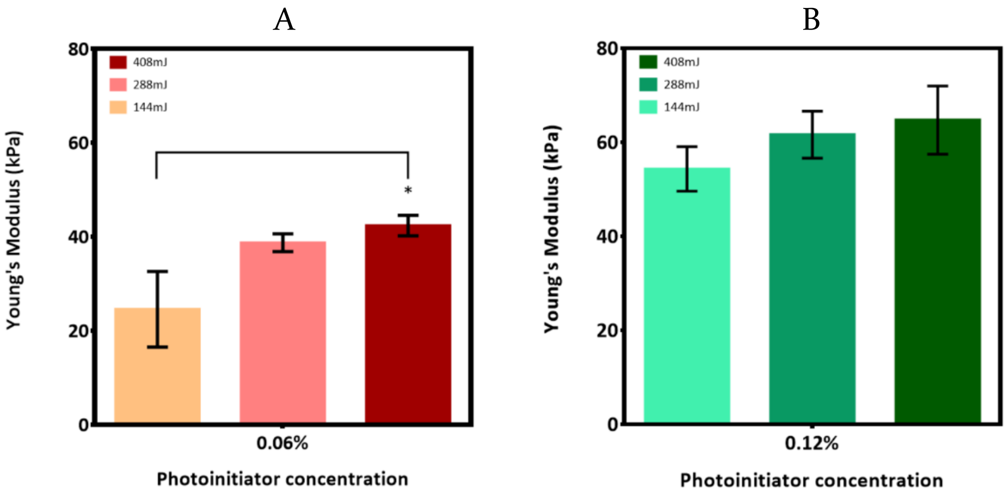

Figure 25 | Indentation data as Young's modulus. Two different concentrations of photoinitiator were used, 0.06 % (left) and 0.12 % (w/v) (right) of LAP, along with three different light energies 144 mJ, 288 mJ and 408 mJ. Data represents mean ± SD (*p ≤ 0.05), where n=3.

This, however, depends on age, hydration and particular area of the body in which measurements are taken, but nonetheless an interesting insight. Holt *et al.* (2008) showed differences in the viscoelastic nature of the dermal and epidermal layers of skin. They concluded that, due to observed strain hardening, the epidermis has more rigid-elastic properties, while the dermis offers a viscous base for ECM support. Thus PTMA hydrogels, with their tailorable physical and mechanical qualities have the potential to be used as a dermal skin layer mimic.

3.5.2 Water uptake

Hydrogels have the capacity to retain large amounts of water or physiological fluids (Ganji *et al.*, 2010). It has previously been indicated that with increased Young's modulus, gelatin hydrogels have a reduction in fluid uptake ability (Zhao *et al.*, 2016). Put simply; fluid retention is inversely proportional to high mechanical properties in some natural hydrogels. This is generally due to the density of crosslinking and polymeric arrangements on a molecular level, which hinder solute penetration (Ganji *et al.*, 2010, Bencherif *et al.*, 2008). The introduction of methacryloyl groups onto polymer backbones tends to reduce the capacity of a hydrogel to swell, for instance, with a high degree of methacrylation, gelMA hydrogels exhibited a reduced degree of swelling (Hoch *et al.*, 2012). In addition to increased steric hindrance as a result of increased level of chemical crosslinking, this could also be ascribed to increased hydrophobicity as a result of substitution with more hydrophobic methacrylate side chains (Chou and Morr, 1979).

The freeze-dried PTMA hydrogels were shown to uptake and retain water over 20–fold of their dry weight at room temperature. This is consistent with previous results (Figure 26) (Morelli and Chiellini, 2010). In other words, this means that the fully hydrated PTMA hydrogels contained > 95% water. A saturation point was reached in both samples prepared at the low and high LAP % in no more than the first 4 hours of hydration.

For the 0.06 % (w/v) sample the equilibrium water uptake was higher than that of the 0.12 % (w/v) LAP. This corresponds directly to the micro-indentation findings, where the former demonstrated weaker mechanical properties.

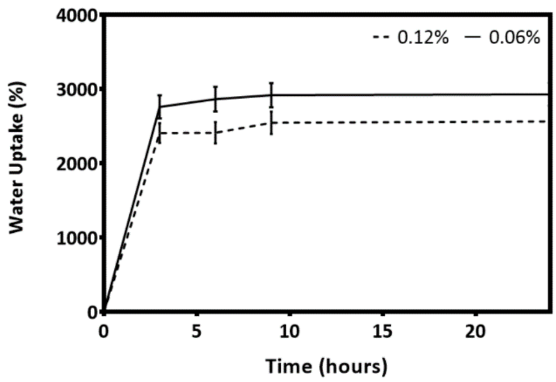

Figure 26 | The water uptake capacity of the photo-crosslinked hydrogels at 288mJ 400nm light. Data represents means ± SD, where n=3.

3.6 Printing and Characterisation

3D printing with a single hydrogel material can be challenging. In this study, the printability of the PTMA ink was manipulated by both physical (discussed in 3.3) and mechanical means.

The determination of strut diameter is a quantitative way to gauge hydrogel print resolution. Strut diameter of printed constructs can be influenced by several factors, including ink and substrate temperature, needle diameter and type (conical vs. cylindrical), print speed and pressure as well as ink viscosity (Chang *et al.*, 2008, Nair *et al.*, 2009). The strut diameter was calculated via image analysis (Figure 27A, B), with varying pressures and print speeds at room temperature. Significant variations in strut size were observed at high pressures with low speed. At a low pressure (2 bar) and speed above 8 mm/s printed fibres gradually became beads, hence strut size was not reported (Appendix).

Printability was significantly impacted by sample temperature, as demonstrated in the rheological temperature sweep. The ink began adhering to the tip at 17 °C at 3 bar and below, resulting in discete droplets rather than strand/filaments (Appendix). At 27 °C dispensed inks began spreading and wilting on the substrate, resulting in strut diameters greater than 1000 μm compromising shape retention (Appendix). Thus, for optimal resolution and processability all scaffold printing was completed at 22 °C.

The strut diameter is fundamental in maintaining the mechanical properties of PTMA hydrogels. Coupled with this is the pore size associated with the scaffold constructs. The pore size of 3D Bioplotted PTMA hydrogels ranged from 506 ± 9.5 µm to 685 ± 31 µm (Figure 27) (Appendix). Pore sizes within the broad range of 100 µm – 600 µm have been shown to be sufficient for cell growth (Rouwkema *et al.*, 2008, Sicchieri *et al.*, 2012). Further, a pore size greater than 300 µm is thought to be suitable for vascularisation (Fedorovich *et al.*, 2011). Interestingly, pore size gradually increased with each layer deposition; this was thought to be associated with amalgamation between each extruded filament. A possible way to overcome this issue would be to cure each layer during the printing process, to ensure shape retention. Alternatively, a reduced substrate and/or reservoir temperature may assist in providing fine resolution, at the expense of increasing the shear forces bestowed upon inks that might be unfavourable for cell bioprinting.

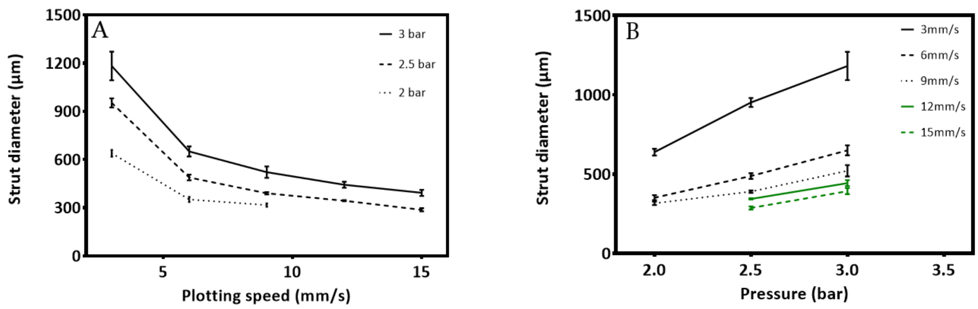

Figure 27 | Average strut diameter of 3D-Bioplotted 9% PTMA hydrogels with a 27-gauge needle (internal diameter of 200 µm) at 22 °C, three different printing pressures were used, 3, 2.5 and 2 bar, along with five different printing speeds, 3, 6, 9, 12 and 15 mm/s. A shows strut diameter as a function of plotting speed and B strut diameter as a function of pressure. Data represents means ± SD, where n=3.

The pore shape can also have a considerable impact on cell growth and differentiation. Laura *et al.* (2016) showed that an increase in porosity resulted in improved seeded cell proliferation of up to 110 %, along with enhancing waste removal and nutrient transport by decreasing diffusion distances (Lewis *et al.*, 2005). This, in turn, leads to more homogeneous cell differentiation (Schuurman *et al.*, 2013) and extracellular matrix deposition (Carrier *et al.*, 2002). Di Luca *et al.* (2016) demonstrated that pore confirmations could dictate cellular differentiation *in vitro*. The found that a decrease in rhomboidal pore geometry from 0 – 15 ° to 0 – 90 ° resulted in an increase in human mesenchymal stem cell chondrogenesis. Scaffold geometry can also influence the mechanical properties of printed constructs (Chien *et al.*, 2013).

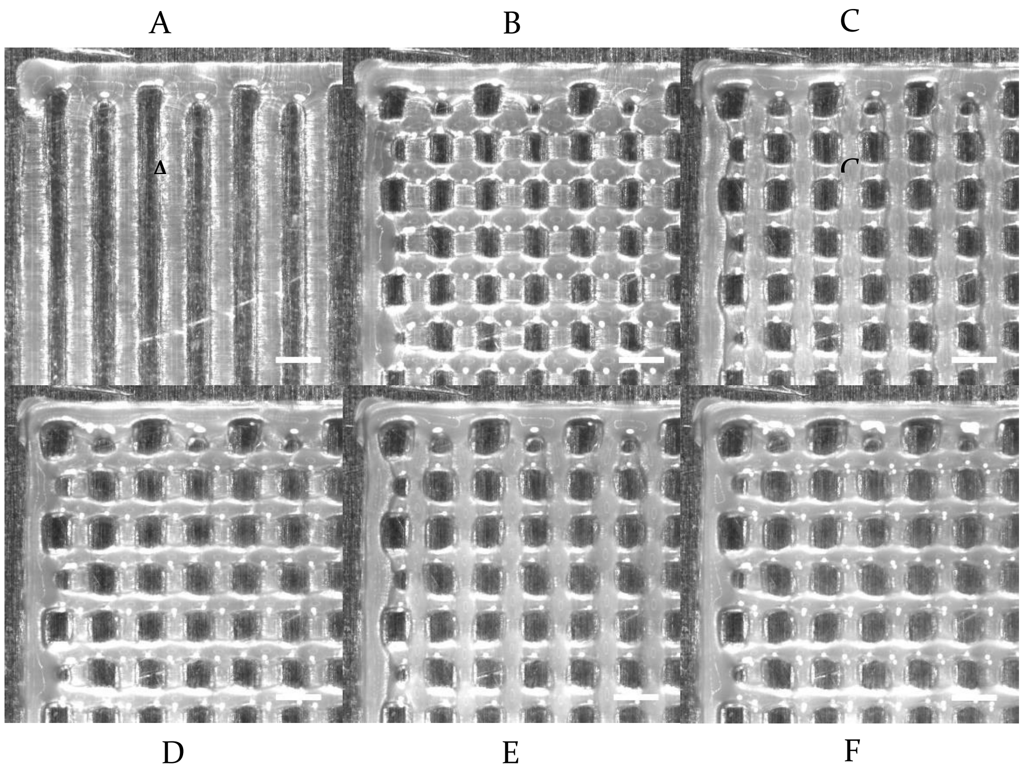

Figure 28 | 6 Layers of PTMA hydrogels printed with the Bioplotter, pressure 2.5 bar, speed 6 mm/s, 22 degrees, cured every second layer for 15 seconds at 408 mJ, then for a further 60 seconds once complete. Images captured with the inbuilt Bioplotter camera at each layer. Layers 1 – 6 are abelled A – F respectively. Scale bar = 1000 µm.

3.7 Cytocompatibility

Preliminary cytocompatibility tests were conducted via *in-vitro* culture of mouse (L929) fibroblast and human adipose-derived stem cells (hASCs) in 3D printed PTMA hydrogels (Figure 29). Both L929 fibroblasts and hASCs showed high cell viability after one day of culture, with negligible cell death detected by live/dead fluorescent staining. Interestingly, both L929 fibroblasts and hASCs demonstrated good attachment and spreading on the 3D printing PTMA hydrogels, with cell morphologies similar to those cultured on tissue culture flasks. This is not seen in plant or bacterially derived hydrogels such as alginate and gellan gum (Lansdown and Payne, 1994).

Cell seeding in pre-fabricated 3D scaffolds can result in poor distribution of cells throughout scaffolds. When cultured in bio-inert hydrogels, cells tend to form

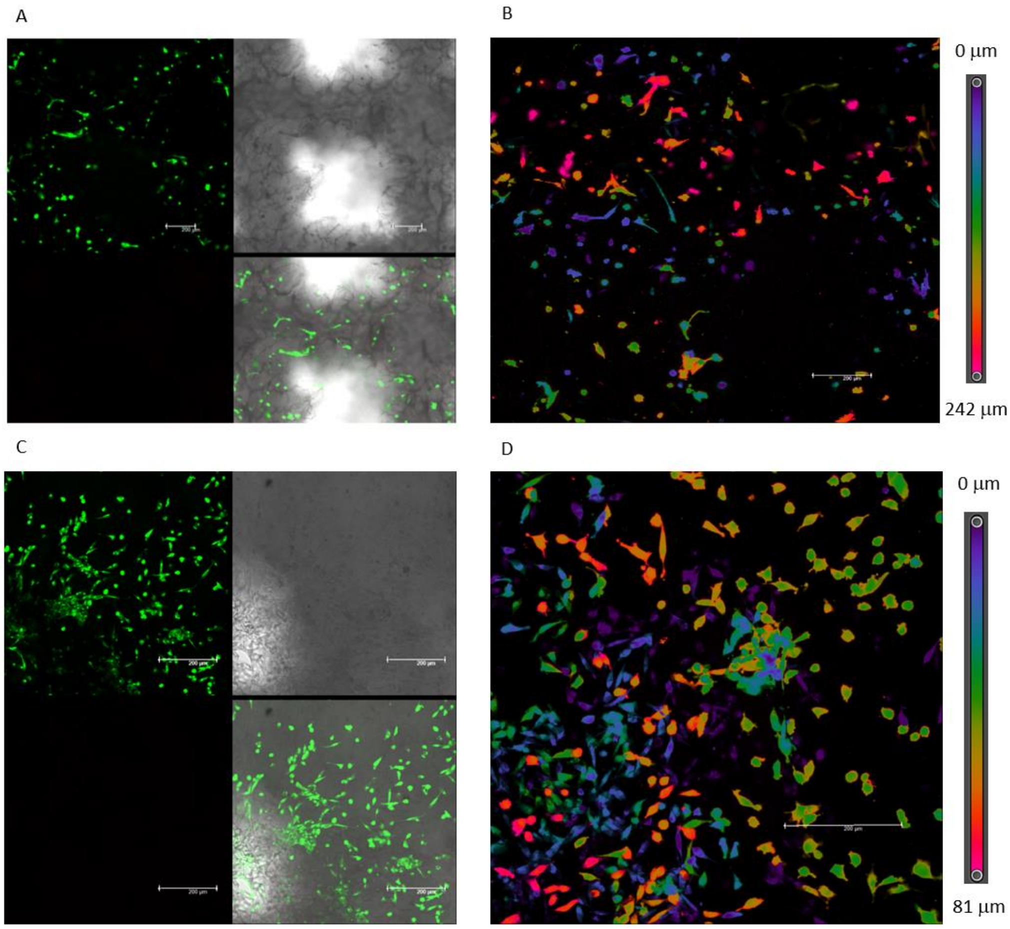

Figure 29 | Laser confocal fluorescence microscopy of hASCs (A) and L929 fibroblasts (C) cultivated in 3D printed PTMA hydrogels for 24 hours, respectively. Cells were stained with calcein AM (for viable cells, green) and propidium iodide (for dead cells, red). (B) and (D) are 3D projections of hASCs and L929 fibroblasts after one day of culture in PTMA scaffolds, respectively showing homogenous dispesions of cells throughout printed scaffolds. Scale bar is 200 µm.

aggregates with rounded morphology (Zhao *et al.*, 2014), typically seen in alginate-based hydrogels (Chayosumrit *et al.*, 2010, Hunt *et al.*, 2010). This is due to lack of adequate cell-matrix interactions. Potential solutions to this are, for example, to modify the alginate-based hydrogels with gelatin (Sarker *et al.*, 2014) or with other cell adhesion moieties or molecules such as RGD or collagen (Prang *et al.*, 2006).

In this study, both hASCs and L929 fibroblast cells demonstrated decent attachment to 3D printed PTMA hydrogels. This warrants an in-depth characterisation, including cell-laden PTMA bioink printing. A number of factors to be examined in the future will be briefly discussed as follows.

For cell printing, appropriately designed bioinks can be used to protect cells from shear stress during extrusion printing through a fine gauge needle (Aguado *et al.*, 2011). This approach will result in improved spatial control of cell distribution, but may have the potential to damage embedded cells (Aguado *et al.*, 2011, Derby, 2012, Pati *et al.*, 2014). Previous work has shown increased cell morphology and hepatocyte formation in soft heparin hydrogels when compared to tough hydrogels, confirming that substrate and ink viscosity and consequent shear stresses are a critical component for tissue development (You *et al.*, 2013). An increase in shear forces has been attributed to reduced cell viability (Nair *et al.*, 2009). Additionally, dense polymeric networks can impact cell migration, as highly viscous bioinks mechanically obstruct cell and nutrient diffusion (Malda *et al.*, 2013, DeForest and Anseth, 2012, Lai *et al.*, 2013, Rutz *et al.*, 2015).

Another important factor to consider is the use of photopolymerisation on cell-laden hydrogels. Both the generation of free radicals and UV light exposure have potentially adverse effects on the encapsulated cells. Literature comparing two cytocompatible photoinitiators, Irgacure 2959 against VA068, shows the latter to be less cytotoxic (Chandler *et al.*, 2011, Rouillard *et al.*, 2011). The LAP photoinitiator used throughout this work has only recently been developed, it exhibits high aqueous solubility and extinction coefficients compared to the aforementioned (Fairbanks *et al.*, 2009). Additionally, LAP can initiate polymerisation under mild visible light illumination with high cell viability (Fairbanks *et al.*, 2009, Lee and Tae, 2007, Bryant *et al.*, 2000). Despite these promising results, further studies focusing on the long-term effects of photo-crosslinking by LAP on cell functions and differentiation are required.

4 CONCLUSIONS

A PT-based bioink was successfully designed through chemical and physical manipulation. Various amounts of unsaturated esters, susceptible to free radical photo-polymerisation, were introduced onto the PT backbone through methacrylation. In doing so, improving the physiological stability of the bioink while maintaining favourable biological functions.

The flow properties of the functionalised physically crosslinked PTMA bioink were found to be suitable for extrusion-based bioprinting. In particular, the inks exhibited both a shear thinning and rapid self-recovery behaviour, which facilitates 3D printing at low extrusion pressures with excellent spatial resolution.

Through manipulating the crosslinking kinetics, the Young's modulus of the PTMA hydrogels began approaching that of the dermal layer of human skin. Additionally, a significant water uptake capacity was observed, suggesting potential use in wound management or as an ECM tissue mimic.

The 3D printed scaffolds were characterised through optical microscopy at differing speeds, pressures and temperatures. This demonstrated the advantages of bioprinting, where strut and pore architecture can be manipulated to suit the application.

Finally, the printed scaffolds were used in a preliminary cytocompatibility study. In culturing human adipose-derived stem cells and mouse L929 fibroblast cells, the PTMA scaffolds showed high cell viability and cell binding affinity.

Through this work, it was uncovered that PT is a prime candidate for use in biofabrication. The exploration of new materials may open up new possibilities in the fabrication of tissues or even organs through bioprinting.

5 FUTURE DIRECTIONS

The potential use of PT in broader biomedical applications is encouraging. Here, for the first time, we fast-tracked PT-based bioink development. Further fundamental studies connecting crosslinking chemistry and molecular associations through the use various photoinitiators, DoF and polymer concentrations to modify the mechanical properties of generated hydrogels or bioinks should be undertaken. Additionally, alternative crosslinking mechanisms could also be explored, including exploitation of carboxyl groups or acrylate functionalisation, to broaden potential applicability of the material. Also, due to the distinct gelling properties of PT, it could be used in drug release and/or the release of specific molecules under certain physicochemical conditions.

Introducing viscosity enhancing polymers such as polyethylene glycol, already used in wound management, glycine,s hyaluronic acid, or gelatin may improve printability and applicability to skin tissue engineering. The introduction of glycerol or glycerin, Newtonian materials, into the PT hydrogel system could advance potential wound healing applications; Elasto-Gel™ a 65% glycerol wound dressing, has been proven to be bacteriostatic and fungistatic (Stout and McKessor, 2012). Glycerol, coupled with hyaluronic acid, has been shown to enhance the printability of bioinks and prevent nozzle clogging (Kang *et al.*, 2016). Additionally, the determination of shear stress bestowed upon the inks during extrusion can be determined. Nair *et al.* (2009) derived a formula to assess the cell viability through a bioprinting system as a function of shear stress.

Future work could explore peptide conjugation and assess the cellular interactions, for targeted applications. Along with the use of different cell types incorporating keratinocytes and dermal fibroblasts, coupled with tailored printing architecture including varying pore size, strut distribution or creating gradients to diversify the tissue mimicking ability of this biomaterial.

6 REFERENCES

ABDEL-FATTAH, A. & EDREES, M. 1973. Seasonal changes in the constituents of Ulva lactuca. *Phytochemistry,* 12, 481-485.

ABE, S., HIRAMATSU, K., ICHIKAWA, O., KAWAMOTO, H., KASAGI, T., MIKI, Y., KIMURA, T. & IKEDA, T. 2013. Safety evaluation of excessive ingestion of mozuku fucoidan in human. *Journal of food science,* 78, T648-T651.

ADLER, S., BASKETTER, D., CRETON, S., PELKONEN, O., VAN BENTHEM, J., ZUANG, V., ANDERSEN, K. E., ANGERS-LOUSTAU, A., APTULA, A. & BAL-PRICE, A. 2011. Alternative (non-animal) methods for cosmetics testing: current status and future prospects—2010. *Archives of toxicology,* 85, 367-485.

AGUADO, B. A., MULYASASMITA, W., SU, J., LAMPE, K. J. & HEILSHORN, S. C. 2011. Improving viability of stem cells during syringe needle flow through the design of hydrogel cell carriers. *Tissue Engineering Part A,* 18, 806-815.

ALVES, A., SOUSA, R. A. & REIS, R. L. 2013. Processing of degradable ulvan 3D porous structures for biomedical applications. *Journal of Biomedical Materials Research - Part A,* 101 A, 998-1006.

ANDREAKIS, N. & SCHAFFELKE, B. 2012. Invasive marine seaweeds: pest or prize? *Seaweed biology.* Springer.

ARAI, K., IWANAGA, S., TODA, H., GENCI, C., NISHIYAMA, Y. & NAKAMURA, M. 2011. Three-dimensional inkjet biofabrication based on designed images. *Biofabrication,* 3, 034113.

ARMOUR, A. D., FISH, J. S., WOODHOUSE, K. A. & SEMPLE, J. L. 2006. A comparison of human and porcine acellularized dermis: interactions with human fibroblasts in vitro. *Plastic and reconstructive surgery,* 117, 845-856.

ATIYEH, B. S., IOANNOVICH, J., AL-AMM, C. A. & EL-MUSA, K. A. 2002. Management of acute and chronic open wounds: the importance of moist environment in optimal wound healing. *Current pharmaceutical biotechnology,* 3, 179-195.

BAKARICH, S. E., PIDCOCK, G. C., BALDING, P., STEVENS, L. & CALVERT, P. 2012. Recovery from applied strain in interpenetrating polymer network hydrogels with ionic and covalent cross-links. *Soft Matter,* 8, 9985-9988.

BANIASADI, M. & MINARY-JOLANDAN, M. 2015. Alginate-collagen fibril composite hydrogel. *Materials,* 8, 799-814.

BARTOLO, P., J., PEREIRA, R., F., BARRIAS, C., C. & GRANJA, P., L. 2013. Advanced biofabrication strategies for skin regeneration and repair. *Nanomedicine*, 603-621.

BÁRTOLO, P. J., DOMINGOS, M., PATRÍCIO, T., COMETA, S. & MIRONOV, V. 2011. Biofabrication strategies for tissue engineering. *Advances on Modeling in Tissue Engineering.* Springer.

BENCHERIF, S. A., SRINIVASAN, A., HORKAY, F., HOLLINGER, J. O., MATYJASZEWSKI, K. & WASHBURN, N. R. 2008. Influence of the degree of methacrylation on hyaluronic acid hydrogels properties. *Biomaterials,* 29, 1739-1749.

BERGER, J., REIST, M., MAYER, J. M., FELT, O. & GURNY, R. 2004. Structure and interactions in chitosan hydrogels formed by complexation or aggregation for biomedical applications. *European Journal of Pharmaceutics and Biopharmaceutics,* 57, 35-52.

BERNFIELD, M., GÖTTE, M., PARK, P. W., REIZES, O., FITZGERALD, M. L., LINCECUM, J. & ZAKO, M. 1999. Functions of cell surface heparan sulfate proteoglycans. *Annual review of biochemistry,* 68, 729-777.

BERTASSONI, L. E., CARDOSO, J. C., MANOHARAN, V., CRISTINO, A. L., BHISE, N. S., ARAUJO, W. A., ZORLUTUNA, P., VRANA, N. E., GHAEMMAGHAMI, A. M. & DOKMECI, M. R. 2014. Direct-write bioprinting of cell-laden methacrylated gelatin hydrogels. *Biofabrication,* 6, 024105.

BHADJA, P., TAN, C.-Y., OUYANG, J.-M. & YU, K. 2016. Repair Effect of Seaweed Polysaccharides with Different Contents of Sulfate Group and Molecular Weights on Damaged HK-2 Cells. *Polymers,* 8, 188.

BILLIET, T., GEVAERT, E., DE SCHRYVER, T., CORNELISSEN, M. & DUBRUEL, P. 2014. The 3D printing of gelatin methacrylamide cell-laden tissue-engineered constructs with high cell viability. *Biomaterials,* 35, 49-62.

BILLIET, T., VANDENHAUTE, M., SCHELFHOUT, J., VAN VLIERBERGHE, S. & DUBRUEL, P. 2012a. A review of trends and limitations in hydrogel-rapid prototyping for tissue engineering. *Biomaterials,* 33, 6020-6041.

BILLIET, T., VANDENHAUTE, M., SCHELFHOUT, J., VAN VLIERBERGHE, S. & DUBRUEL, P. 2012b. Review: A review of trends and limitations in hydrogel-rapid prototyping for tissue engineering. *Biomaterials,* 33, 6020-6041.

BLAESER, A., DUARTE CAMPOS, D. F., PUSTER, U., RICHTERING, W., STEVENS, M. M. & FISCHER, H. 2015. Controlling Shear Stress in 3D Bioprinting is a Key Factor to Balance Printing Resolution and Stem Cell Integrity. *Advanced healthcare materials*.

BOHANDY, J., KIM, B. & ADRIAN, F. 1986. Metal deposition from a supported metal film using an excimer laser. *Journal of Applied Physics,* 60, 1538-1539.

BONDOC, C. & BURKE, J. 1971. Clinical experience with viable frozen human skin and a frozen skin bank. *Annals of surgery,* 174, 371.

BÖTTCHER-HABERZETH, S., BIEDERMANN, T. & REICHMANN, E. 2010. Tissue engineering of skin. *Burns,* 36, 450-460.

BRADING, J. W., GEORG-PLANT, M. & HARDY, D. M. 1954. The polysaccharide from the alga Ulva lactuca. Purification, hydrolysis, and methylation of the polysaccharide. *Journal of the Chemical Society (Resumed)*, 319-324.

BRANNON-PEPPAS, L. & PEPPAS, N. A. 1991. Equilibrium swelling behavior of pH-sensitive hydrogels. *Chemical Engineering Science,* 46, 715-722.

BREASTED, J. H. 1930. *The Edwin Smith Surgical Papyrus: published in facsimile and hieroglyphic transliteration with translation and commentary in two volumes*, Chic. UP.

BRYANT, S. J., DAVIS-AREHART, K. A., LUO, N., SHOEMAKER, R. K., ARTHUR, J. A. & ANSETH, K. S. 2004. Synthesis and characterization of photopolymerized multifunctional hydrogels: water-soluble poly (vinyl alcohol) and chondroitin sulfate macromers for chondrocyte encapsulation. *Macromolecules,* 37, 6726-6733.

BRYANT, S. J., NUTTELMAN, C. R. & ANSETH, K. S. 2000. Cytocompatibility of UV and visible light photoinitiating systems on cultured NIH/3T3 fibroblasts in vitro. *Journal of Biomaterials Science, Polymer Edition,* 11, 439-457.

BURKE, J. F., YANNAS, I. V., QUINBY JR, W. C., BONDOC, C. C. & JUNG, W. K. 1981. Successful use of a physiologically acceptable artificial skin in the treatment of extensive burn injury. *Annals of surgery,* 194, 413.

CAI, C., GUO, Z., YANG, Y., GENG, Z., TANG, L., ZHAO, M., QIU, Y., CHEN, Y. & HE, P. 2016. Inhibition of Hydrogen Peroxide induced Injuring on Human Skin Fibroblast by Ulva prolifera Polysaccharide. *International Journal of Biological Macromolecules*.

CALVERT, P. 2001. Inkjet printing for materials and devices. *Chemistry of materials,* 13, 3299-3305.

CALVERT, P. 2007. Printing cells. *Science,* 318, 208-209.

CARRIER, R. L., RUPNICK, M., LANGER, R., SCHOEN, F. J., FREED, L. E. & VUNJAK-NOVAKOVIC, G. 2002. Perfusion improves tissue architecture of engineered cardiac muscle. *Tissue engineering,* 8, 175-188.

CATHAL, D., DI BELLA, C., THOMPSON, F., AUGUSTINE, C., BEIRNE, S., CORNOCK, R., RICHARDS, C. J., CHUNG, J., GAMBHIR, S. & YUE, Z. 2016. Development of the Biopen: a handheld device for surgical printing of adipose stem cells at a chondral wound site. *Biofabrication,* 8, 015019.

CAZANDER, G., JUKEMA, G. N. & NIBBERING, P. H. 2012. Complement activation and inhibition in wound healing. *Clinical and Developmental Immunology,* 2012.

CHANDIKA, P., KO, S. C. & JUNG, W. K. 2015. Marine-derived biological macromolecule-based biomaterials for wound healing and skin tissue regeneration. *Int J Biol Macromol,* 77, 24-35.

CHANDLER, E. M., BERGLUND, C. M., LEE, J. S., POLACHECK, W. J., GLEGHORN, J. P., KIRBY, B. J. & FISCHBACH, C. 2011. Stiffness of photocrosslinked RGD-alginate gels regulates adipose progenitor cell behavior. *Biotechnology and bioengineering,* 108, 1683-1692.

CHANG, R., NAM, J. & SUN, W. 2008. Effects of dispensing pressure and nozzle diameter on cell survival from solid freeform fabrication-based direct cell writing. *Tissue Engineering Part A,* 14, 41-48.

CHARDACK, W. M., MARTIN, M. M., JEWETT, T. C. & BOYER, B. E. 1962. Synthetic substitutes for skin: Clinical Experience with Their Use in the Treatment of Burns. *Plastic and Reconstructive Surgery,* 30, 554-567.

CHAYOSUMRIT, M., TUCH, B. & SIDHU, K. 2010. Alginate microcapsule for propagation and directed differentiation of hESCs to definitive endoderm. *Biomaterials,* 31, 505-514.

CHIELLINI, F. & MORELLI, A. 2011. Ulvan: a versatile platform of biomaterials from renewable resources. *Biomaterials- Physics and Chemistry*.

CHIEN, K. B., MAKRIDAKIS, E. & SHAH, R. N. 2013. Three-dimensional printing of soy protein scaffolds for tissue regeneration. *Tissue Eng Part C Methods,* 19, 417-26.

CHOU, D. H. & MORR, C. V. 1979. Protein-water interactions and functional properties. *Journal of the American oil chemists' Society,* 56, A53-A62.

CLARK, R. A., GHOSH, K. & TONNESEN, M. G. 2007. Tissue engineering for cutaneous wounds. *Journal of Investigative Dermatology,* 127, 1018-1029.

COOPER, R., DRAGAR, C., ELLIOT, K., FITTON, J., GODWIN, J. & THOMPSON, K. 2002. GFS, a preparation of Tasmanian Undaria pinnatifida is associated with healing and inhibition of reactivation of Herpes. *BMC complementary and alternative medicine,* 2, 11.

COSTA, L., FIDELIS, G., CORDEIRO, S., OLIVEIRA, R., SABRY, D., CÂMARA, R., NOBRE, L., COSTA, M., ALMEIDA-LIMA, J. & FARIAS, E. 2010. Biological activities of sulfated polysaccharides from tropical seaweeds. *Biomedicine & Pharmacotherapy,* 64, 21-28.

COUTINHO, D. F., SANT, S. V., SHIN, H., OLIVEIRA, J. T., GOMES, M. E., NEVES, N. M., KHADEMHOSSEINI, A. & REIS, R. L. 2010. Modified Gellan Gum hydrogels with tunable physical and mechanical properties. *Biomaterials,* 31, 7494-7502.

CROWTHER, M., BROWN, N., BISHOP, E. & LEWIS, C. 2001. Microenvironmental influence on macrophage regulation of angiogenesis in wounds and malignant tumors. *Journal of Leukocyte Biology,* 70, 478-490.

CUI, X., BOLAND, T., D D'LIMA, D. & K LOTZ, M. 2012. Thermal inkjet printing in tissue engineering and regenerative medicine. *Recent patents on drug delivery & formulation,* 6, 149-155.

CUNHA, L. & GRENHA, A. 2016. Sulfated Seaweed Polysaccharides as Multifunctional Materials in Drug Delivery Applications. *Marine drugs,* 14, 42.

DAI, N.-T., WILLIAMSON, M., KHAMMO, N., ADAMS, E. & COOMBES, A. 2004. Composite cell support membranes based on collagen and polycaprolactone for tissue engineering of skin. *Biomaterials,* 25, 4263-4271.

DAMONTE, E. B., MATULEWICZ, M. C. & CEREZO, A. S. 2004. Sulfated seaweed polysaccharides as antiviral agents. *Curr Med Chem,* 11, 2399-419.

DANION, F., VARRAINE, E., BONNARD, M. & PAILHOUS, J. 2003. Stride variability in human gait: the effect of stride frequency and stride length. *Gait Posture,* 18, 69-77.

DASH, M., SAMAL, S. K., BARTOLI, C., MORELLI, A., SMET, P. F., DUBRUEL, P. & CHIELLINI, F. 2014. Biofunctionalization of ulvan scaffolds for bone tissue engineering. *ACS Appl Mater Interfaces,* 6, 3211-8.

DAVOODI, P., FENG, F., XU, Q., YAN, W.-C., TONG, Y. W., SRINIVASAN, M., SHARMA, V. K. & WANG, C.-H. 2015. Coaxial electrohydrodynamic atomization: Microparticles for drug delivery applications. *Journal of Controlled Release,* 205, 70-82.

DE COPPI, P., BARTSCH, G., JR., SIDDIQUI, M. M., XU, T., SANTOS, C. C., PERIN, L., MOSTOSLAVSKY, G., SERRE, A. C., SNYDER, E. Y., YOO, J. J., FURTH, M. E., SOKER, S. & ATALA, A. 2007. Isolation of amniotic stem cell lines with potential for therapy. *Nat Biotechnol,* 25, 100-6.

DE FREITAS, M. B., FERREIRA, L. G., HAWERROTH, C., DUARTE, M. E. R., NOSEDA, M. D. & STADNIK, M. J. 2015. Ulvans induce resistance against

plant pathogenic fungi independently of their sulfation degree. *Carbohydrate Polymers,* 133, 384-390.
DEFOREST, C. A. & ANSETH, K. S. 2012. Advances in bioactive hydrogels to probe and direct cell fate. *Annual review of chemical and biomolecular engineering,* 3, 421-444.
DERBY, B. 2008. Bioprinting: inkjet printing proteins and hybrid cell-containing materials and structures. *Journal of Materials Chemistry,* 18, 5717-5721.
DERBY, B. 2010. Inkjet printing of functional and structural materials: fluid property requirements, feature stability, and resolution. *Annual Review of Materials Research,* 40, 395-414.
DERBY, B. 2012. Printing and prototyping of tissues and scaffolds. *Science,* 338, 921-926.
DI LUCA, A., LORENZO-MOLDERO, I., MOTA, C., LEPEDDA, A., AUHL, D., VAN BLITTERSWIJK, C. & MORONI, L. 2016. Tuning Cell Differentiation into a 3D Scaffold Presenting a Pore Shape Gradient for Osteochondral Regeneration. *Advanced healthcare materials*.
DIEGEL, O., REAY, S., SINGAMNENI, S. & WITHELL, A. 2010. Tools for sustainable product design: additive manufacturing.
DRAGET, K. I., SKJÅK-BRÆK, G. & SMIDSRØD, O. 1997. Alginate based new materials. *International journal of biological macromolecules,* 21, 47-55.
EMING, S. A., KRIEG, T. & DAVIDSON, J. M. 2007. Inflammation in wound repair: molecular and cellular mechanisms. *Journal of Investigative Dermatology,* 127, 514-525.
ESKO, J. D. & LINHARDT, R. J. 2009. Proteins that Bind Sulfated Glycosaminoglycans. *In:* VARKI, A., CUMMINGS, R. D., ESKO, J. D., FREEZE, H. H., STANLEY, P., BERTOZZI, C. R., HART, G. W. & ETZLER, M. E. (eds.) *Essentials of Glycobiology.* Cold Spring Harbor (NY): Cold Spring Harbor Laboratory Press

The Consortium of Glycobiology Editors, La Jolla, California.
FAIRBANKS, B. D., SCHWARTZ, M. P., BOWMAN, C. N. & ANSETH, K. S. 2009. Photoinitiated polymerization of PEG-diacrylate with lithium phenyl-2,4,6-trimethylbenzoylphosphinate: polymerization rate and cytocompatibility. *Biomaterials,* 30, 6702-6707.
FALKOWSKI, P. G., BARBER, R. T. & SMETACEK, V. 1998. Biogeochemical controls and feedbacks on ocean primary production. *Science,* 281, 200-206.
FARIAS, E. H., POMIN, V. H., VALENTE, A.-P., NADER, H. B., ROCHA, H. A. & MOURÃO, P. A. 2008. A preponderantly 4-sulfated, 3-linked galactan from the green alga Codium isthmocladum. *Glycobiology,* 18, 250-259.
FARLEY, C. T. & GONZALEZ, O. 1996. Leg stiffness and stride frequency in human running. *J Biomech,* 29, 181-6.
FEDOROVICH, N. E., ALBLAS, J., HENNINK, W. E., ÖNER, F. C. & DHERT, W. J. 2011. Organ printing: the future of bone regeneration? *Trends in biotechnology,* 29, 601-606.
FERRIS, C. J., GILMORE, K. G. & WALLACE, G. G. 2013. Biofabrication: an overview of the approaches used for printing of living cells. *Applied microbiology and biotechnology,* 97, 4243-4258.

FIELD, C. K. & KERSTEIN, M. D. 1994. Overview of wound healing in a moist environment. *The American journal of surgery,* 167, S2-S6.
GALLICO III, G. G., O'CONNOR, N. E., COMPTON, C. C., KEHINDE, O. & GREEN, H. 1984. Permanent coverage of large burn wounds with autologous cultured human epithelium. *New England Journal of Medicine,* 311, 448-451.
GANJI, F., VASHEGHANI-FARAHANI, S. & VASHEGHANI-FARAHANI, E. 2010. Theoretical description of hydrogel swelling: a review. *Iran Polym J,* 19, 375-398.
GAO, J., CRAPO, P. M. & WANG, Y. 2006. Macroporous elastomeric scaffolds with extensive micropores for soft tissue engineering. *Tissue engineering,* 12, 917-925.
GECKIL, H., XU, F., ZHANG, X., MOON, S. & DEMIRCI, U. 2010. Engineering hydrogels as extracellular matrix mimics. *Nanomedicine,* 5, 469-484.
GEHRKE, S. H., FISHER, J. P., PALASIS, M. & LUND, M. E. 1997. Factors determining hydrogel permeability. *Annals of the New York Academy of Sciences,* 831, 179-184.
GIBSON, I., ROSEN, D. W. & STUCKER, B. 2010. *Additive manufacturing technologies*, Springer.
GONG, J. P., KATSUYAMA, Y., KUROKAWA, T. & OSADA, Y. 2003. Double-network hydrogels with extremely high mechanical strength. *Advanced Materials,* 15, 1155-1158.
GRAVES, N. & ZHENG, H. 2014. Modelling the direct health care costs of chronic wounds in Australia.
GRIMM, A. T. 2004. *User's Guide to Rapid Prototyping*, Society of Manufacturing Engineers (SME).
GRUENE, M., UNGER, C., KOCH, L., DEIWICK, A. & CHICHKOV, B. 2011. Dispensing pico to nanolitre of a natural hydrogel by laser-assisted bioprinting. *Biomedical engineering online,* 10, 1.
GUTMANN, A. K., JACOBI, B., BUTCHER, M. T. & BERTRAM, J. E. 2006. Constrained optimization in human running. *J Exp Biol,* 209, 622-32.
HACHET, E., VAN DEN BERGHE, H., BAYMA, E., BLOCK, M. R. & AUZELY-VELTY, R. 2012. *Design of Biomimetic Cell-Interactive Substrates Using Hyaluronic Acid Hydrogels with Tunable Mechanical Properties*.
HANSON SHEPHERD, J. N., PARKER, S. T., SHEPHERD, R. F., GILLETTE, M. U., LEWIS, J. A. & NUZZO, R. G. 2011. 3D microperiodic hydrogel scaffolds for robust neuronal cultures. *Advanced functional materials,* 21, 47-54.
HAUG, A. 1976. The influence of borate and calcium on the gel formation of a sulfated polysaccharide from Ulva lactuca. *Acta chemica Scandinavica. Series B: Organic chemistry and biochemistry,* 30, 562-566.
HOCH, E., HIRTH, T., TOVAR, G. E. & BORCHERS, K. 2013. Chemical tailoring of gelatin to adjust its chemical and physical properties for functional bioprinting. *Journal of Materials Chemistry B,* 1, 5675-5685.
HOCH, E., SCHUH, C., HIRTH, T., TOVAR, G. E. & BORCHERS, K. 2012. Stiff gelatin hydrogels can be photo-chemically synthesized from low viscous gelatin solutions using molecularly functionalized gelatin with a high degree of methacrylation. *Journal of Materials Science: Materials in Medicine,* 23, 2607-2617.

HOCKADAY, L. A., KANG, K. H., COLANGELO, N. W., CHEUNG, P. Y., DUAN, B., MALONE, E., WU, J., GIRARDI, L. N., BONASSAR, L. J., LIPSON, H., CHU, C. C. & BUTCHER, J. T. 2012. Rapid 3D printing of anatomically accurate and mechanically heterogeneous aortic valve hydrogel scaffolds. *Biofabrication,* 4, 035005.

HOFFMAN, A. S. 2012. Hydrogels for biomedical applications. *Advanced drug delivery reviews,* 64, 18-23.

HOLT, B., TRIPATHI, A. & MORGAN, J. 2008. Viscoelastic response of human skin to low magnitude physiologically relevant shear. *Journal of biomechanics,* 41, 2689-2695.

HUANG, C.-Y., WU, S.-J., YANG, W.-N., KUAN, A.-W. & CHEN, C.-Y. 2015. Antioxidant activities of crude extracts of fucoidan extracted from Sargassum glaucescens by a compressional-puffing-hydrothermal extraction process. *Food Chemistry*.

HUEBSCH, N., LIPPENS, E., LEE, K., MEHTA, M., KOSHY, S. T., DARNELL, M. C., DESAI, R. M., MADL, C. M., XU, M. & ZHAO, X. 2015. Matrix elasticity of void-forming hydrogels controls transplanted-stem-cell-mediated bone formation. *Nature materials,* 14, 1269-1277.

HULL, C. W. 1986. Apparatus for production of three-dimensional objects by stereolithography. Google Patents.

HUNT, N., SMITH, A. M., GBURECK, U., SHELTON, R. & GROVER, L. 2010. Encapsulation of fibroblasts causes accelerated alginate hydrogel degradation. *Acta Biomaterialia,* 6, 3649-3656.

HUNT, T. K. 1988. The physiology of wound healing. *Annals of emergency medicine,* 17, 1265-1273.

HUTMACHER, D. W. 2000. Scaffolds in tissue engineering bone and cartilage. *Biomaterials,* 21, 2529-2543.

JAKAB, K., DAMON, B., NEAGU, A., KACHURIN, A. & FORGACS, G. 2006. Three-dimensional tissue constructs built by bioprinting. *Biorheology,* 43, 509-513.

JIAO, G., YU, G., ZHANG, J. & EWART, H. S. 2011. Chemical structures and bioactivities of sulfated polysaccharides from marine algae. *Marine Drugs,* 9, 196-223.

JOHNSON, F. A., CRAIG, D. Q. & MERCER, A. D. 1997. Characterization of the block structure and molecular weight of sodium alginates. *Journal of pharmacy and pharmacology,* 49, 639-643.

JOHNSON, K. L. 1985. In Contact Mechanics *Cambridge University Press, Cambridge* 69, 214.

JUNGST, T., SMOLAN, W., SCHACHT, K., SCHEIBEL, T. & GROLL, J. 2016. Strategies and Molecular Design Criteria for 3D Printable Hydrogels. *Chemical Reviews,* 116, 1496-1539.

KAEFFER, B., BÉNARD, C., LAHAYE, M., BLOTTIERE, H. M. & CHERBUT, C. 1999. Biological properties of ulvan, a new source of green seaweed sulfated polysaccharides, on cultured normal and cancerous colonic epithelial cells. *Planta medica,* 65, 527-531.

KANDHASAMY, M. & ARUNACHALAM, K. 2008. Evaluation of in vitro antibacterial property of seaweeds of southeast coast of India. *African Journal of Biotechnology,* 7.

KANG, H.-W., LEE, S. J., KO, I. K., KENGLA, C., YOO, J. J. & ATALA, A. 2016. A 3D bioprinting system to produce human-scale tissue constructs with structural integrity. *Nature biotechnology,* 34, 312-319.

KANNO, K. 2012. Biocompatible Hydrogel from a Green Tide-Forming Chiorophyta. *Journal of Sustainable Development,* 5, 38.

KERIQUEL, V., GUILLEMOT, F., ARNAULT, I., GUILLOTIN, B., MIRAUX, S., AMÉDÉE, J., FRICAIN, J.-C. & CATROS, S. 2010. In vivo bioprinting for computer-and robotic-assisted medical intervention: preliminary study in mice. *Biofabrication,* 2, 014101.

KHALIL, S. & SUN, W. 2007. Biopolymer deposition for freeform fabrication of hydrogel tissue constructs. *Materials Science and Engineering: C,* 27, 469-478.

KHALIL, S. & SUN, W. 2009. Bioprinting endothelial cells with alginate for 3D tissue constructs. *Journal of biomechanical engineering,* 131, 111002.

KIETZMANN, J., PITT, L. & BERTHON, P. 2015. Disruptions, decisions, and destinations: Enter the age of 3-D printing and additive manufacturing. *Business Horizons,* 58, 209-215.

KIRKER, K., LUO, Y., MORRIS, S., SHELBY, J. & PRESTWICH, G. 2004. Glycosaminoglycan hydrogels as supplemental wound dressings for donor sites. *Journal of Burn Care & Research,* 25, 276-286.

KLOXIN, A. M., KASKO, A. M., SALINAS, C. N. & ANSETH, K. S. 2009. Photodegradable hydrogels for dynamic tuning of physical and chemical properties. *Science,* 324, 59-63.

KOCH, L., KUHN, S., SORG, H., GRUENE, M., SCHLIE, S., GAEBEL, R., POLCHOW, B., REIMERS, K., STOELTING, S., MA, N., VOGT, P. M., STEINHOFF, G. & CHICHKOV, B. 2010. Laser printing of skin cells and human stem cells. *Tissue Eng Part C Methods,* 16, 847-54.

KOKSHENEV, V. B. 2004. Dynamics of human walking at steady speeds. *Phys Rev Lett,* 93, 208101.

KOLESKY, D. B., TRUBY, R. L., GLADMAN, A., BUSBEE, T. A., HOMAN, K. A. & LEWIS, J. A. 2014. 3D bioprinting of vascularized, heterogeneous cell-laden tissue constructs. *Advanced materials,* 26, 3124-3130.

KONNO, T. & ISHIHARA, K. 2007. Temporal and spatially controllable cell encapsulation using a water-soluble phospholipid polymer with phenylboronic acid moiety. *Biomaterials,* 28, 1770-1777.

LAHAYE, M. & AXELOS, M. 1993. Gelling properties of water-soluble polysaccharides from proliferating marine green seaweeds (Ulva spp.). *Carbohydrate polymers,* 22, 261-265.

LAHAYE, M. & RAY, B. 1996. Cell-wall polysaccharides from the marine green alga Ulva “rigida”(Ulvales, Chlorophyta)—NMR analysis of ulvan oligosaccharides. *Carbohydrate research,* 283, 161-173.

LAHAYE, M. & ROBIC, A. 2007. Structure and functional properties of ulvan, a polysaccharide from green seaweeds. *Biomacromolecules,* 8, 1765-74.

LAI, J.-Y., MA, D. H.-K., LAI, M.-H., LI, Y.-T., CHANG, R.-J. & CHEN, L.-M. 2013. Characterization of cross-linked porous gelatin carriers and their interaction with corneal endothelium: Biopolymer concentration effect. *PloS one,* 8, e54058.

LANGER, R. & VACANTI, J. P. 1993. Tissue engineering. *Science,* 260, 920-6.
LANSDOWN, A. & PAYNE, M. 1994. An evaluation of the local reaction and biodegradation of calcium sodium alginate (Kaltostat) following subcutaneous implantation in the rat. *Journal of the Royal College of Surgeons of Edinburgh,* 39, 284-288.
LAURA, R.-C., ANDREW, G., CALLUM, F., JOEL, S., KEVIN, S. & JING, Y. 2016. Characterisation of the surface structure of 3D printed scaffolds for cell infiltration and surgical suturing. *Biofabrication,* 8, 015016.
LEE, J.-B., HAYASHI, K., MAEDA, M. & HAYASHI, T. 2004. Antiherpetic activities of sulfated polysaccharides from green algae. *Planta medica,* 70, 813-817.
LEE, K. Y. & MOONEY, D. J. 2001. Hydrogels for tissue engineering. *Chemical reviews,* 101, 1869-1880.
LEE, S.-Y. & TAE, G. 2007. Formulation and in vitro characterization of an in situ gelable, photo-polymerizable Pluronic hydrogel suitable for injection. *Journal of controlled release,* 119, 313-319.
LEE, W., DEBASITIS, J. C., LEE, V. K., LEE, J.-H., FISCHER, K., EDMINSTER, K., PARK, J.-K. & YOO, S.-S. 2009. Multi-layered culture of human skin fibroblasts and keratinocytes through three-dimensional freeform fabrication. *Biomaterials,* 30, 1587-1595.
LEWIS, M. C., MACARTHUR, B. D., MALDA, J., PETTET, G. & PLEASE, C. P. 2005. Heterogeneous proliferation within engineered cartilaginous tissue: the role of oxygen tension. *Biotechnology and bioengineering,* 91, 607-615.
LI, H., LIU, S. & LIN, L. 2016. Rheological study on 3D printability of alginate hydrogel and effect of graphene oxide. *International Journal of Bioprinting,* 2.
LIANG, H. C., CHANG, W. H., LIANG, H. F., LEE, M. H. & SUNG, H. W. 2004. Crosslinking structures of gelatin hydrogels crosslinked with genipin or a water-soluble carbodiimide. *Journal of Applied Polymer Science,* 91, 4017-4026.
LIANG, X. & BOPPART, S. A. 2010. Biomechanical properties of in vivo human skin from dynamic optical coherence elastography. *IEEE Transactions on Biomedical Engineering,* 57, 953-959.
LIN, C.-C. & ANSETH, K. S. 2009. PEG hydrogels for the controlled release of biomolecules in regenerative medicine. *Pharmaceutical research,* 26, 631-643.
LODE, A., KRUJATZ, F., BRÜGGEMEIER, S., QUADE, M., SCHÜTZ, K., KNAACK, S., WEBER, J., BLEY, T. & GELINSKY, M. 2015. Green bioprinting: Fabrication of photosynthetic algae-laden hydrogel scaffolds for biotechnological and medical applications. *Engineering in Life Sciences,* 15, 177-183.
LÜ, J. M., LIN, P. H., YAO, Q. & CHEN, C. 2010. Chemical and molecular mechanisms of antioxidants: experimental approaches and model systems. *Journal of cellular and molecular medicine,* 14, 840-860.
MACNEIL, S. 2007. Progress and opportunities for tissue-engineered skin. *Nature,* 445, 874-880.

MALDA, J., VISSER, J., MELCHELS, F. P., JÜNGST, T., HENNINK, W. E., DHERT, W. J., GROLL, J. & HUTMACHER, D. W. 2013. 25th anniversary article: engineering hydrogels for biofabrication. *Advanced Materials,* 25, 5011-5028.

MANIVASAGAN, P. & OH, J. 2016. Marine polysaccharide-based nanomaterials as a novel source of nanobiotechnological applications. *International Journal of Biological Macromolecules,* 82, 315-327.

MARKSTEDT, K., MANTAS, A., TOURNIER, I., MARTÍNEZ ÁVILA, H. C., HÄGG, D. & GATENHOLM, P. 2015. 3D bioprinting human chondrocytes with nanocellulose–alginate bioink for cartilage tissue engineering applications. *Biomacromolecules,* 16, 1489-1496.

MATLOUB, A. A., ELSOUDA, S. S. M., EL-SENOUSY, W. M., HAMED, M., ALY, H., ALI, S. A., MOHAMMED, R. S., MAHMOUD, K., EL-HALLOUTY, S. & IBRAHIM, N. A. 2015. In vitro Antiviral, Cytotoxic, Antioxidant and Hypolipidemic Activites of Polysaccharide Isolated From Marine Algae.

MATTOX, J. M. 2013. Additive Manufacturing and its Implications for Military Ethics. *Journal of Military Ethics,* 12, 225-234.

MCKEE, C. T., LAST, J. A., RUSSELL, P. & MURPHY, C. J. 2011. Indentation versus tensile measurements of Young's modulus for soft biological tissues. *Tissue Engineering Part B: Reviews,* 17, 155-164.

MCNALLY, W. D. & RUST, C. 1928. The distribution of boric acid in human organs in six deaths due to boric acid poisoning. *Journal of the American Medical Association,* 90, 382-383.

MELCHELS, F. P., DHERT, W. J., HUTMACHER, D. W. & MALDA, J. 2014. Development and characterisation of a new bioink for additive tissue manufacturing. *Journal of Materials Chemistry B,* 2, 2282-2289.

METCALFE, A. D. & FERGUSON, M. W. 2007a. Bioengineering skin using mechanisms of regeneration and repair. *Biomaterials,* 28, 5100-5113.

METCALFE, A. D. & FERGUSON, M. W. 2007b. Tissue engineering of replacement skin: the crossroads of biomaterials, wound healing, embryonic development, stem cells and regeneration. *Journal of the Royal Society Interface,* 4, 413-437.

MEZGER, T. G. 2006. *The rheology handbook: for users of rotational and oscillatory rheometers,* Vincentz Network GmbH & Co KG.

MICHAEL, M., JANA, B., MATTHIAS, S. & MARCY, Z.-W. 2015. Nanostructured Pluronic hydrogels as bioinks for 3D bioprinting. *Biofabrication,* 7, 035006.

MICHAEL, S., SORG, H., PECK, C.-T., KOCH, L., DEIWICK, A., CHICHKOV, B., VOGT, P. M. & REIMERS, K. 2013. Tissue engineered skin substitutes created by laser-assisted bioprinting form skin-like structures in the dorsal skin fold chamber in mice. *PloS one,* 8, e57741.

MIHAILA, S. M., GAHARWAR, A. K., REIS, R. L., MARQUES, A. P., GOMES, M. E. & KHADEMHOSSEINI, A. 2013. Photocrosslinkable Kappa-Carrageenan Hydrogels for Tissue Engineering Applications. *Advanced healthcare materials,* 2, 895-907.

MIYAGAWA, S., HIROSE, H., SHIRAKURA, R., NAKA, Y., NAKATA, S., KAWASHIMA, Y., SEYA, T., MATSUMOTO, M., UENAKA, A. & KITAMURA, H. 1988. The mechanism of discordant xenograft rejection. *Transplantation,* 46, 825-829.

MONDY, W. L., CAMERON, D., TIMMERMANS, J.-P., DE CLERCK, N., SASOV, A., CASTELEYN, C. & PIEGL, L. A. 2009. Computer-aided design of microvasculature systems for use in vascular scaffold production. *Biofabrication,* 1, 035002.

MOOREFIELD, E. C., MCKEE, E. E., SOLCHAGA, L., ORLANDO, G., YOO, J. J., WALKER, S., FURTH, M. E. & BISHOP, C. E. 2011. Cloned, CD117 selected human amniotic fluid stem cells are capable of modulating the immune response. *PLoS One,* 6, e26535.

MORELLI, A., BETTI, M., PUPPI, D., BARTOLI, C., GAZZARRI, M. & CHIELLINI, F. 2015. Enzymatically Crosslinked Ulvan Hydrogels as Injectable Systems for Cell Delivery. *Macromolecular Chemistry and Physics*.

MORELLI, A. & CHIELLINI, F. 2010. Ulvan as a New Type of Biomaterial from Renewable Resources: Functionalization and Hydrogel Preparation. *Macromolecular Chemistry and Physics,* 211, 821-832.

MURPHY, S. V. & ATALA, A. 2014. 3D bioprinting of tissues and organs. *Nat Biotechnol,* 32, 773-85.

NAFICY, S., KAWAKAMI, S., SADEGHOLVAAD, S., WAKISAKA, M. & SPINKS, G. M. 2013. Mechanical properties of interpenetrating polymer network hydrogels based on hybrid ionically and covalently crosslinked networks. *Journal of Applied Polymer Science,* 130, 2504-2513.

NAIR, K., GANDHI, M., KHALIL, S., YAN, K. C., MARCOLONGO, M., BARBEE, K. & SUN, W. 2009. Characterization of cell viability during bioprinting processes. *Biotechnol. J,* 4, 1168-1177.

NAKAMURA, M., IWANAGA, S., HENMI, C., ARAI, K. & NISHIYAMA, Y. 2010. Biomatrices and biomaterials for future developments of bioprinting and biofabrication. *Biofabrication,* 2, 014110.

NIKKHAH, M., ESHAK, N., ZORLUTUNA, P., ANNABI, N., CASTELLO, M., KIM, K., DOLATSHAHI-PIROUZ, A., EDALAT, F., BAE, H. & YANG, Y. 2012. Directed endothelial cell morphogenesis in micropatterned gelatin methacrylate hydrogels. *Biomaterials,* 33, 9009-9018.

O'CONNOR, N., MULLIKEN, J., BANKS-SCHLEGEL, S., KEHINDE, O. & GREEN, H. 1981. Grafting of burns with cultured epithelium prepared from autologous epidermal cells. *The Lancet,* 317, 75-78.

OYEN, M. 2014. Mechanical characterisation of hydrogel materials. *International Materials Reviews,* 59, 44-59.

PARK, J. E. & BARBUL, A. 2004. Understanding the role of immune regulation in wound healing. *The American Journal of Surgery,* 187, S11-S16.

PARZEL, C. A., PEPPER, M. E., BURG, T., GROFF, R. E. & BURG, K. J. 2009. EDTA enhances high-throughput two-dimensional bioprinting by inhibiting salt scaling and cell aggregation at the nozzle surface. *J Tissue Eng Regen Med,* 3, 260-8.

PASQUI, D., DE CAGNA, M. & BARBUCCI, R. 2012. Polysaccharide-based hydrogels: the key role of water in affecting mechanical properties. *Polymers,* 4, 1517-1534.

PATI, F., JANG, J., HA, D.-H., KIM, S. W., RHIE, J.-W., SHIM, J.-H., KIM, D.-H. & CHO, D.-W. 2014. Printing three-dimensional tissue analogues with decellularized extracellular matrix bioink. *Nature communications,* 5.

PAUL, W. & SHARMA, C. P. 2004. Chitosan and alginate wound dressings: a short review. *Trends Biomater Artif Organs,* 18, 18-23.

PAUS, R. & COTSARELIS, G. 1999. The biology of hair follicles. *New England Journal of Medicine,* 341, 491-497.

PECK, M. D. 2011. Epidemiology of burns throughout the world. Part I: Distribution and risk factors. *Burns,* 37, 1087-1100.

PENGZHAN, Y., NING, L., XIGUANG, L., GEFEI, Z., QUANBIN, Z. & PENGCHENG, L. 2003. Antihyperlipidemic effects of different molecular weight sulfated polysaccharides from Ulva pertusa (Chlorophyta). *Pharmacological Research,* 48, 543-549.

PETERSEN, R. C. 2012. Reactive secondary sequence oxidative pathology polymer model and antioxidant tests. *International research journal of pure and applied chemistry,* 2, 247.

PLATT, J. L., FISCHEL, R. J., MATAS, A. J., REIF, S. A., BOLMAN, R. M. & BACH, F. H. 1991. Immunopathology of hyperacute xenograft rejection in a swine-to-primate model. *Transplantation,* 52, 214-220.

PRANG, P., MULLER, R., ELJAOUHARI, A., HECKMANN, K., KUNZ, W., WEBER, T., FABER, C., VROEMEN, M., BOGDAHN, U. & WEIDNER, N. 2006. The promotion of oriented axonal regrowth in the injured spinal cord by alginate-based anisotropic capillary hydrogels. *Biomaterials,* 27, 3560-9.

PRUNIÉRAS, M., RÉGNIER, M. & WOODLEY, D. 1983. Methods for cultivation of keratinocytes with an air-liquid interface. *Journal of Investigative Dermatology,* 81.

QI, H., ZHANG, Q., ZHAO, T., CHEN, R., ZHANG, H., NIU, X. & LI, Z. 2005. Antioxidant activity of different sulfate content derivatives of polysaccharide extracted from Ulva pertusa (Chlorophyta) in vitro. *International Journal of Biological Macromolecules,* 37, 195-199.

QIAO, L., LI, Y., CHI, Y., JI, Y., GAO, Y., HWANG, H., AKER, W. G. & WANG, P. 2016. Rheological properties, gelling behavior and texture characteristics of polysaccharide from Enteromorpha prolifera. *Carbohydrate polymers,* 136, 1307-1314.

QIN, S., LIN, H. & JIANG, P. 2012. Advances in genetic engineering of marine algae. *Biotechnology advances,* 30, 1602-1613.

QUEMENER, B., LAHAYE, M. & BOBIN-DUBIGEON, C. 1997. Sugar determination in ulvans by a chemical-enzymatic method coupled to high performance anion exchange chromatography. *Journal of Applied Phycology,* 9, 179-188.

RALSTON, D. L., C; DALLEY, A; BOYCE, S; FREELANDER, E; MAC NEIL, S. 1999. The requirement for basement membrane antigens in the production of human epidermal/dermal composites in vitro. *British Journal of Dermatology,* 140, 605-615.

RAPRAEGER, A. C. 1993. The coordinated regulation of heparan sulfate, syndecans and cell behavior. *Current opinion in cell biology,* 5, 844-853.

RATNER, B. D., HOFFMAN, A. S., SCHOEN, F. J. & LEMONS, J. E. 2004. *Biomaterials science: an introduction to materials in medicine,* Academic press.

RAY, B. & LAHAYE, M. 1995. Cell-wall polysaccharides from the marine green alga Ulva "rigida"(Ulvales, Chlorophyta). Extraction and chemical composition. *Carbohydrate Research,* 274, 251-261.

REYS, L. L., SILVA, S. S., SOARES DA COSTA, D. P., OLIVEIRA, N. M., MANO, J. F., REIS, R. L. & SILVA, T. H. 2016. Fucoidan hydrogels photocrosslinked with visible radiation as matrices for cell culture. *ACS Biomaterials Science & Engineering*.

RHEINWALD, J. G. & GREEN, H. 1977. Epidermal growth factor and the multiplication of cultured human epidermal keratinocytes. *Nature,* 265, 421-424.

RHEINWATD, J. G. & GREEN, H. 1975. Seria cultivation of strains of human epidemal keratinocytes: the formation keratinizin colonies from single cell is. *Cell,* 6, 331-343.

RINGEISEN, B. R., KIM, H., BARRON, J. A., KRIZMAN, D. B., CHRISEY, D. B., JACKMAN, S., AUYEUNG, R. & SPARGO, B. J. 2004. Laser printing of pluripotent embryonal carcinoma cells. *Tissue engineering,* 10, 483-491.

ROBIC, A., GAILLARD, C., SASSI, J. F., LERAT, Y. & LAHAYE, M. 2009a. Ultrastructure of ulvan: a polysaccharide from green seaweeds. *Biopolymers,* 91, 652-64.

ROBIC, A., RONDEAU-MOURO, C., SASSI, J. F., LERAT, Y. & LAHAYE, M. 2009b. Structure and interactions of ulvan in the cell wall of the marine green algae Ulva rotundata (Ulvales, Chlorophyceae). *Carbohydrate Polymers,* 77, 206-216.

ROBIC, A., SASSI, J.-F., DION, P., LERAT, Y. & LAHAYE, M. 2009c. SEASONAL VARIABILITY OF PHYSICOCHEMICAL AND RHEOLOGICAL PROPERTIES OF ULVAN IN TWO ULVA SPECIES (CHLOROPHYTA) FROM THE BRITTANY COAST. *Journal of Phycology,* 45, 962-973.

ROBSON, S. C., SCHULTE, J. & BACH, F. H. 1999. Factors in xenograft rejection. *Annals of the New York Academy of Sciences,* 875, 261-276.

ROUILLARD, A. D., BERGLUND, C. M., LEE, J. Y., POLACHECK, W. J., TSUI, Y., BONASSAR, L. J. & KIRBY, B. J. 2011. Methods for photocrosslinking alginate hydrogel scaffolds with high cell viability. *Tissue Engineering. Part C, Methods,* 17, 173-179.

ROUWKEMA, J., RIVRON, N. C. & VAN BLITTERSWIJK, C. A. 2008. Vascularization in tissue engineering. *Trends in biotechnology,* 26, 434-441.

ROWLEY, J. A., MADLAMBAYAN, G. & MOONEY, D. J. 1999. Alginate hydrogels as synthetic extracellular matrix materials. *Biomaterials,* 20, 45-53.

RUTZ, A. L., HYLAND, K. E., JAKUS, A. E., BURGHARDT, W. R. & SHAH, R. N. 2015. A Multimaterial Bioink Method for 3D Printing Tunable, Cell-Compatible Hydrogels. *Advanced Materials,* 27, 1607-1614.

SARKER, B., SINGH, R., SILVA, R., ROETHER, J. A., KASCHTA, J., DETSCH, R., SCHUBERT, D. W., CICHA, I. & BOCCACCINI, A. R. 2014. Evaluation of fibroblasts adhesion and proliferation on alginate-gelatin crosslinked hydrogel. *PLoS One,* 9, e107952.

SCARANO, A., CARINCI, F. & PIATTELLI, A. 2009. Lip augmentation with a new filler (agarose gel): a 3-year follow-up study. *Oral Surg Oral Med Oral Pathol Oral Radiol Endod,* 108, e11-5.

SCHIELE, N. R., CHRISEY, D. B. & CORR, D. T. 2010a. Gelatin-based laser direct-write technique for the precise spatial patterning of cells. *Tissue Engineering Part C: Methods,* 17, 289-298.

SCHIELE, N. R., CORR, D. T., HUANG, Y., RAOF, N. A., XIE, Y. & CHRISEY, D. B. 2010b. Laser-based direct-write techniques for cell printing. *Biofabrication,* 2, 032001.

SCHILLINGER, B. M., BERSTEIN, M., GOLDBERG, L. A. & SHALITA, A. R. 1982. Boric acid poisoning. *Journal of the American Academy of Dermatology,* 7, 667-673.

SCHUURMAN, W., LEVETT, P. A., POT, M. W., VAN WEEREN, P. R., DHERT, W. J., HUTMACHER, D. W., MELCHELS, F. P., KLEIN, T. J. & MALDA, J. 2013. Gelatin-Methacrylamide Hydrogels as Potential Biomaterials for Fabrication of Tissue-Engineered Cartilage Constructs. *Macromolecular bioscience,* 13, 551-561.

SHANTHA, K. & HARDING, D. 2002. Synthesis and evaluation of sucrose-containing polymeric hydrogels for oral drug delivery. *Journal of applied polymer science,* 84, 2597-2604.

SHAO, P., QIN, M., HAN, L. & SUN, P. 2014. Rheology and characteristics of sulfated polysaccharides from chlorophytan seaweeds Ulva fasciata. *Carbohydrate polymers,* 113, 365-372.

SHARIATI, S. R. P. & MOEINZADEH, S. 2015. Hydrogels for Cell Encapsulation and Bioprinting. *Bioprinting in Regenerative Medicine.* Springer.

SICCHIERI, L. G., CRIPPA, G. E., DE OLIVEIRA, P. T., BELOTI, M. M. & ROSA, A. L. 2012. Pore size regulates cell and tissue interactions with PLGA–CaP scaffolds used for bone engineering. *Journal of tissue engineering and regenerative medicine,* 6, 155-162.

SINGH, B., FLEURY, C., JALALVAND, F. & RIESBECK, K. 2012. Human pathogens utilize host extracellular matrix proteins laminin and collagen for adhesion and invasion of the host. *FEMS microbiology reviews,* 36, 1122-1180.

SINNO, H. & PRAKASH, S. 2013. Complements and the wound healing cascade: an updated review. *Plastic surgery international,* 2013.

SKARDAL, A., MACK, D., KAPETANOVIC, E., ATALA, A., JACKSON, J. D., YOO, J. & SOKER, S. 2012. Bioprinted Amniotic Fluid-Derived Stem Cells Accelerate Healing of Large Skin Wounds. *Stem Cells Translational Medicine,* 1, 792-802.

SKARDAL, A., ZHANG, J., MCCOARD, L., XU, X., OOTTAMASATHIEN, S. & PRESTWICH, G. D. 2010. Photocrosslinkable hyaluronan-gelatin hydrogels for two-step bioprinting. *Tissue Engineering. Part A,* 16, 2675-2685.

SOHAL, R. S. & SOHAL, B. H. 1991. Hydrogen peroxide release by mitochondria increases during aging. *Mech Ageing Dev,* 57, 187-202.

STEVENS, M. M. 2008. Biomaterials for bone tissue engineering. *Materials today,* 11, 18-25.

STOKES, J. R. 2011. Rheology of industrially relevant microgels. *Microgel Suspensions: Fundamentals and Applications*, 327-353.

STOUT, E. I. & MCKESSOR, A. 2012. Glycerin-Based Hydrogel for Infection Control. *Advances in Wound Care,* 1, 48-51.

STRACCIA, M. C., D'AYALA, G. G., ROMANO, I., OLIVA, A. & LAURIENZO, P. 2015. Alginate hydrogels coated with chitosan for wound dressing. *Mar Drugs,* 13, 2890-908.

SUN, J.-Y., ZHAO, X., ILLEPERUMA, W. R., CHAUDHURI, O., OH, K. H., MOONEY, D. J., VLASSAK, J. J. & SUO, Z. 2012. Highly stretchable and tough hydrogels. *Nature,* 489, 133-136.

SWIFT, M. E., KLEINMAN, H. K. & DIPIETRO, L. A. 1999. Impaired wound repair and delayed angiogenesis in aged mice. *Laboratory investigation; a journal of technical methods and pathology,* 79, 1479-1487.

TAMMI, R., JANSÉN, C. T. & SANTTI, R. 1979. Histometric analysis of human skin in organ culture. *Journal of Investigative Dermatology,* 73, 138-140.

TEKIN, E., SMITH, P. J. & SCHUBERT, U. S. 2008. Inkjet printing as a deposition and patterning tool for polymers and inorganic particles. *Soft Matter,* 4, 703-713.

TOBIN, D. J. 2006. Biochemistry of human skin—our brain on the outside. *Chemical Society Reviews,* 35, 52-67.

TOIDA, T., AMORNRUT, C. & LINHARDT, R. J. 2003. Structure and bioactivity of sulfated polysaccharides. *Trends in Glycoscience and Glycotechnology,* 15, 29-46.

TOSKAS, G., HUND, R.-D., LAOURINE, E., CHERIF, C., SMYRNIOTOPOULOS, V. & ROUSSIS, V. 2011. Nanofibers based on polysaccharides from the green seaweed Ulva rigida. *Carbohydrate Polymers,* 84, 1093-1102.

UNGER, C., GRUENE, M., KOCH, L., KOCH, J. & CHICHKOV, B. N. 2011. Time-resolved imaging of hydrogel printing via laser-induced forward transfer. *Applied Physics A,* 103, 271-277.

VARSHNEY, L. 2007. Role of natural polysaccharides in radiation formation of PVA–hydrogel wound dressing. *Nuclear Instruments and Methods in Physics Research Section B: Beam Interactions with Materials and Atoms,* 255, 343-349.

WANG, L.-F., SHEN, S.-S. & LU, S.-C. 2003. Synthesis and characterization of chondroitin sulfate–methacrylate hydrogels. *Carbohydrate Polymers,* 52, 389-396.

WEBBER, R. E. & SHULL, K. R. 2004. Strain dependence of the viscoelastic properties of alginate hydrogels. *Macromolecules,* 37, 6153-6160.

WELLER, C. & SUSSMAN, G. 2006. Wound dressings update. *Journal of pharmacy practice and research,* 36, 318-324.

WIGGER-ALBERTI, W., KUHLMANN, M., EKANAYAKE, S., WILHELM, D., BUETTNER, H., CALLAGHAN, T. & WILHELM, K. 2009. Using a novel wound model to investigate the healing properties of products for superficial wounds. *Journal of wound care,* 18, 123-131.

WINTER, G. D. 1962. Formation of the scab and the rate of epithelization of superficial wounds in the skin of the young domestic pig.

XU, T., GREGORY, C. A., MOLNAR, P., CUI, X., JALOTA, S., BHADURI, S. B. & BOLAND, T. 2006. Viability and electrophysiology of neural cell structures generated by the inkjet printing method. *Biomaterials,* 27, 3580-3588.

YANG, F., WANG, J., PENG, G., FU, S., ZHANG, S. & LIU, C. 2012. PEG-based bioresponsive hydrogels with redox-mediated formation and degradation. *J Mater Sci Mater Med,* 23, 697-710.

YANNAS, I. & BURKE, J. F. 1980. Design of an artificial skin. I. Basic design principles. *Journal of biomedical materials research,* 14, 65-81.

YOU, J., PARK, S.-A., SHIN, D.-S., PATEL, D., RAGHUNATHAN, V. K., KIM, M., MURPHY, C. J., TAE, G. & REVZIN, A. 2013. Characterizing the effects of heparin gel stiffness on function of primary hepatocytes. *Tissue Engineering Part A,* 19, 2655-2663.

YUK, H., ZHANG, T., PARADA, G. A., LIU, X. & ZHAO, X. 2016. Skin-inspired hydrogel-elastomer hybrids with robust interfaces and functional microstructures. *Nat Commun,* 7.

ZHAO, X., LANG, Q., YILDIRIMER, L., LIN, Z. Y., CUI, W., ANNABI, N., NG, K. W., DOKMECI, M. R., GHAEMMAGHAMI, A. M. & KHADEMHOSSEINI, A. 2016. Photocrosslinkable gelatin hydrogel for epidermal tissue engineering. *Advanced healthcare materials,* 5, 108-118.

ZHAO, Y., YAO, R., OUYANG, L., DING, H., ZHANG, T., ZHANG, K., CHENG, S. & SUN, W. 2014. Three-dimensional printing of Hela cells for cervical tumor model in vitro. *Biofabrication,* 6, 035001.

ZORLUTUNA, P., VRANA, N. E. & KHADEMHOSSEINI, A. 2013. The expanding world of tissue engineering: the building blocks and new applications of tissue engineered constructs. *IEEE reviews in biomedical engineering,* 6, 47-62.

7 APPENDIX

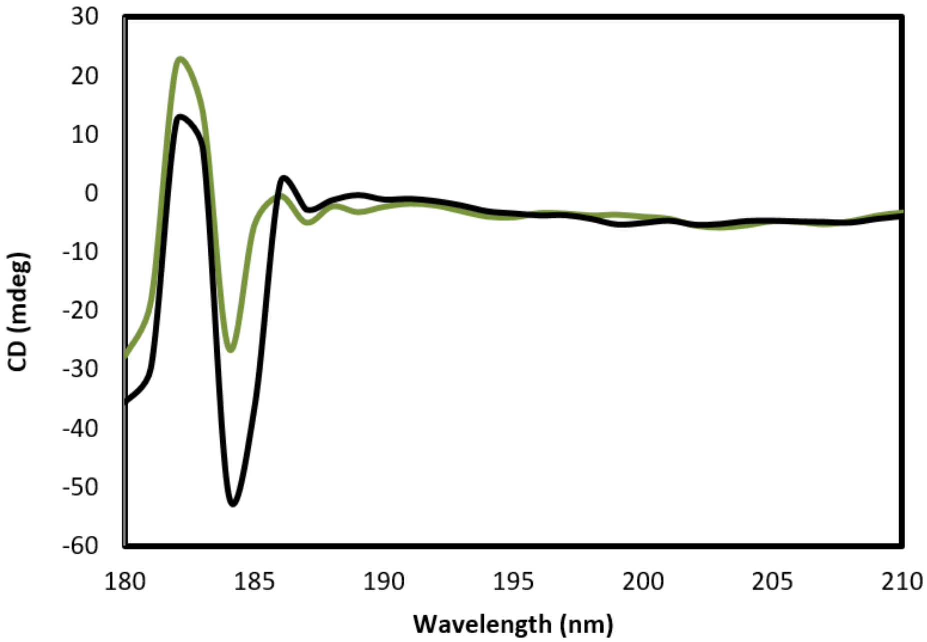

Figure 30 | Circular dichroism of native PT (black) and PTMA10 (green), both 0.1 % solutions in water.

Table 5 | Raw *in-situ* rheology crosslinking kinetics of both low and high photoinitiator concentrations with significant difference summary.

Tukey's multiple comparisons test	Mean Diff.	95% CI of diff.	Significance	Summary
0.06%:15 vs. 0.06%:30	-14.16	-28.88 to 0.5603	No	ns
0.06%:15 vs. 0.06%:45	-17.8	-32.53 to -3.082	Yes	*
0.06%:15 vs. 0.12%:15	-29.74	-44.46 to -15.02	Yes	***
0.06%:15 vs. 0.12%:30	-37.04	-51.76 to -22.31	Yes	****
0.06%:15 vs. 0.12%:45	-40.14	-54.86 to -25.41	Yes	****
0.06%:30 vs. 0.06%:45	-3.642	-18.36 to 11.08	No	ns
0.06%:30 vs. 0.12%:15	-15.58	-30.30 to -0.8557	Yes	*
0.06%:30 vs. 0.12%:30	-22.88	-37.60 to -8.153	Yes	**
0.06%:30 vs. 0.12%:45	-25.98	-40.70 to -11.25	Yes	***
0.06%:45 vs. 0.12%:15	-11.94	-26.66 to 2.786	No	ns
0.06%:45 vs. 0.12%:30	-19.23	-33.96 to -4.511	Yes	**
0.06%:45 vs. 0.12%:45	-22.33	-37.06 to -7.611	Yes	**
0.12%:15 vs. 0.12%:30	-7.297	-22.02 to 7.425	No	ns
0.12%:15 vs. 0.12%:45	-10.4	-25.12 to 4.325	No	ns
0.12%:30 vs. 0.12%:45	-3.1	-17.82 to 11.62	No	ns

Table 6 | Strut diameter raw data from imaging analysis. The average values are given ± the standard deviation, where n = 3. NB '*' indicates failed extrusion and consequent droplet formation (instead of continual lines) and '–' indicates failed strut structural retention.

Print speed	Strut diameter (µm)								
	17 °C			22 °C			27 °C		
	2 bar	2.5 bar	3 bar	2 bar	2.5 bar	3 bar	2 bar	2.5 bar	3 bar

3 mm/s	378 ± 0.03	484 ± 0.02	581 ± 0.02	639 ± 21	952 ± 28	1182 ± 89	1360 ± 0.06	-	-
6 mm/s	*	332 ± 0.01	333 ± 0.02	352 ± 16	488 ± 18	650 ± 31	1158 ± 0.04	-	-
9 mm/s	*	*	300 ± 0.02	317 ± 11	390 ± 7.1	522 ± 35	1012 ± 0.07	-	-
12 mm/s	*	*	*	*	344 ± 3.7	433 ± 19	959 ± 0.06	-	-
15 mm/s	*	*	*	*	287 ± 10	393 ± 19	921 ± 0.06	-	-

Table 7 | Raw scaffold architecture data quantified with ImageJ. Where n=5. Refer to 2.6 to gauge how measurements were taken.

Layer	Horizontal strut		Vertical strut		Pore width		Max pore distance	
	Average	SD	Average	SD	Average	SD	Average	SD
2	302	17.56132113	483.6	29.35029812	506.248	9.52334059	719.4	14.58218
3	328.6	10.26839812	440.4	12.81561547	619.6	21.32228881	670.2	18.42173
4	292.4	16.11955334	373.8	12.63962025	637	14.12798641	678.8	17.53169
5	293.8	13.21211565	362.8	10.38075142	672.6	22.59734498	638.2	18.11519
	258.8	21.90342439	326.6	18.62900964	684.8	31.30111819	661	14.05703